minerals

MDPI

Article

Formation of Diagenetic Minerals in the Carboniferous Rock Complex from the Fore-Sudetic Monocline (SW Poland): Fluid Inclusion, Isotopic and Raman Constraints

Aleksandra Kozłowska, Katarzyna Jarmołowicz-Szulc *, Marta Kuberska and Krystyna Wołkowicz

Polish Geological Institute—National Research Institute, Rakowiecka 4, 00-975 Warsaw, Poland; aleksandra.kozlowska@pgi.gov.pl (A.K.); marta.kuberska@pgi.gov.pl (M.K.); krystyna.wolkowicz@pgi.gov.pl (K.W.)

* Correspondence: kjar@pgi.gov.pl; Tel.: +48-691745191

Abstract: The paper presents the latest state of knowledge on clastic sedimentary rocks from the Carboniferous complex in the SW part of the Polish Lowlands, studied to help determine their potential prospectivity for the occurrence of oil and/or gas deposits. Rocks were analyzed with respect to the petrographic-mineralogical characteristics of the Carboniferous deposits, their diagenesis, determinations of pressure-temperature conditions of mineral formation and the hydrocarbon occurrence. Analyses were carried out on samples from four selected boreholes in the Fore-Sudetic Monocline. After microscopic analysis of rocks and minerals in thin sections, the following techniques were used: luminescence analysis (UV, blue light), microthermometric analysis of fluid inclusions in double-sided polished wafers, cathodoluminescence analysis, electron scanning microscope studies, XRD analyses, stable isotopic analyses (carbon, oxygen) on calcite and dolomite-ankerite and Raman spectra of fluid inclusions. Orthochemical components, such as carbonates and authigenic quartz, that form cements or fill the veins cutting the sample material have been studied. Fluid inclusion data in quartz and carbonates result in homogenization temperatures of 74–233 °C. The Raman analysis gives temperature estimations for the organic matter of about 164 °C and 197 °C, depending on the borehole, which points to a low coalification degree. The post-sedimentary processes of compaction, cementation and diagenetic dissolution under eo- and meso-diagenetic conditions to temperatures of over 160 °C influenced the present character of the deposits. P-T conditions of brines and methane trapping have been estimated to be ~850–920 bars and 185–210 °C (vein calcite) and ~1140 bars and 220 °C (Fe-dolomite/ankerite). Therefore, locally, temperatures might have been higher (>200 °C), which may be a symptom of local regional metamorphism of a very low degree.

Keywords: diagenesis; clastic rocks; carbonates; fluid inclusions; isotopes; Carboniferous

Citation: Kozłowska, A.; Jarmołowicz-Szulc, K.; Kuberska, M.; Wołkowicz, K. Formation of Diagenetic Minerals in the Carboniferous Rock Complex from the Fore-Sudetic Monocline (SW Poland): Fluid Inclusion, Isotopic and Raman Constraints. *Minerals* **2021**, *11*, 976. https://doi.org/10.3390/min11090976

Academic Editors: Georgia Pe-Piper and Stephen E. Laubach

Received: 4 June 2021
Accepted: 2 September 2021
Published: 7 September 2021

1. Introduction

Carboniferous deposits in the Fore-Sudetic Monocline have been under study since the 70s of the 20th century. Most lithological, stratigraphic, petrographic and petrophysical analyses were conducted during borehole logging (e.g., [1,2]). Petrographic characteristics of the Carboniferous rocks are shown by [3] and references therein, among others. Only a few papers deal with post-depositional processes [4–6]. A newer interpretation of the petrographic results for the Carboniferous sandstones is presented by [7], being followed by [8].

The Carboniferous clastic deposits in the Wielkopolska-Silesian zone, mainly in the Wielkoposka area [9], are Mississippian and Pennsylvanian in age. They were penetrated by over a dozen boreholes (Figure 1). Recently, these deposits have been again the object of interest of research projects [10,11]. The aim of these projects has been deepening and supplementing the knowledge of unconventional hydrocarbon systems in Poland.

Sandstones that occur in the Wielkopolska-Silesian zone are of interest as prospective reservoirs. Schistose sandstones co-occurring with siltstones may contain gas and represent a source of the tight gas accumulated in the sandstones [12].

In the present paper, the results of the first stable isotopic analyses (carbon, oxygen) in carbonate minerals and Raman analyses in these deposits are presented. Fluid inclusion (FI) research in authigenic quartz and carbonates was conducted, and the results are compared to data published earlier by [4,13,14]. As it has been widely discussed in the literature, e.g., [15–17], FI microthermometry and isotope analyses may lead to the reconstruction of primary conditions of mineral formation, and to composition and density of the paleofluids in the sedimentary basin [18,19].

The combination of these new data with a petrographic analysis enables better recognition of the diagenetic evolution of the Carboniferous deposits in the Fore-Sudetic Monocline.

2. Geological Setting

The Carboniferous deposits in the bottom of the Fore-Sudetic Monocline and west of the Upper Silesia area belong to the outer part of the Variscan orogen, interpreted to be the Moravia- Silesian and Wielkopolska externides [20]. The deep-sea flysch sediments of the Culm facies were deposited in the Tournasian and Visean. The Sudetes were presumably a source of sedimentary material for these deposits. The material was transported toward the NW and W [20]. In the Namurian, the deepest part of the basin with a deposition of the Culmian flysch sediments, was narrowed to the northern and eastern parts of the Fore-Sudetic Monocline. Shallow marine clastics were most likely deposited in the marginal parts of the basin. The Variscan orogeny caused an uplift of W and S Poland resulting in exhumation of the Fore-Sudetic basement during the Westphalian and Stephanian [21].

Tectonic deformation of the Carboniferous deposits and associated flysch complexes resulted in the formation of folds and nappes [22]. The mesostructural analyses of the drill log showed abundant tectonic structures, such as fissures [23,24]. Many fissures are sub-vertical and are healed with calcite, dolomite, clay minerals and iron oxides. The tectonic and regional studies of [25] show that tectonic deformations are more common in the upper parts compared to the lower parts of the sections. The stratigraphic studies point to the occurrence of the Carboniferous deposits of age from Tournaisian to Stephanian (among others: [26,27], and references therein).

Most boreholes in SW Poland only drilled the upper parts of the Carboniferous series (Figure 1). Only some boreholes reach deeper but not to the bottom of the system.

The top of the Carboniferous deposits lies at a depth of ~1.6 km (Więcki IG 1) to over 4.8 km (Września IG1). The succession of Carboniferous rocks consists of alternating claystones, mudstones, sandstones and locally conglomerates of a total thickness from several hundred meters to some thousands [28].

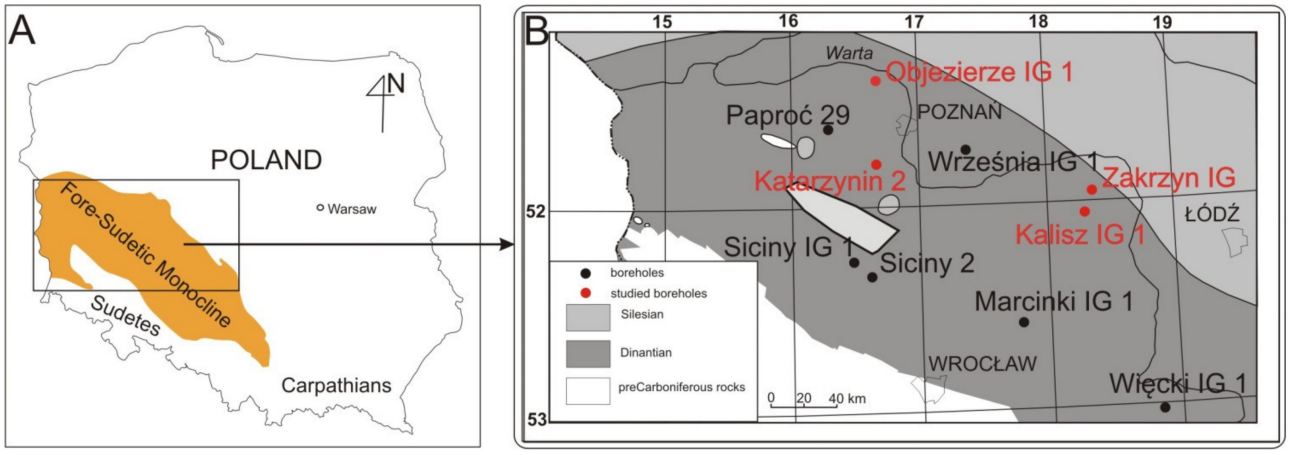

Figure 1. (**A**) The location of Fore-Sudetic Monocline; (**B**) A map of the top of the Carboniferous (according to [29]) with the locations of the studied boreholes.

3. Materials and Methods

The studied rocks come from four boreholes: Kalisz IG 1, Katarzynin 2, Objezierze IG 1 and Zakrzyn IG 1, situated in the north-western part of the Fore-Sudetic Monocline (Figure 1).

Petrographic analyses were conducted on one hundred forty-three thin sections using the Optiphot 2 Pol (Nikon) polarization microscope. Samples were prepared from the rocks saturated with a blue resin to allow pore percentage determinations. Microlithofacial characteristics of sandstones were based on the classification of [30]. To assist the determination of types of the carbonates, uncovered thin sections with the carbonates were stained with Evamy's solution.

Cathodoluminescence analysis (CL) was performed on all the samples using an English CCL 8200 mk3 equipment with a cold cathode produced by Cambridge Image Technology Ltd. combined with a Nikon Optiphot microscope. CL observations were used in the analysis of detrital material and cement and the textural features of the rocks, as well.

Studies with a 1430 LEO electron scanning microscope with EDS and ISIS were conducted on forty-nine samples. Based on the observation of rock chips covered with carbon, and gold, the minerals filling the pore space were determined. Twenty-eight analyses of the chemical composition of the carbonates in micro-areas were performed on eight uncovered polished samples using VSP and SEM QUANT programs.

X-ray analyses were performed using two types of equipment. Thirty qualitative and quantitative analyses were performed using the X-ray diffractometer X'Pert PW 3020 by Philips (Polish Geological Institute, Warsaw). The phase analysis was conducted on powder samples (grains to 0.063 mm). Diffractograms were registered at angle interval of 5° ÷ 60° 2θ and identified based on ICDD tests. The composition of clay fraction (<0.02 mm) was determined using oriented samples in the air-dry stage after glycolization and heating (550 °C). Quantitative measurements of 50 samples were performed using X'Pert Pro equipment produced by Panalytical with an X'Celerator counter (Institute for Oil and Gas, Cracow). The following conditions were used: excitation voltage of 40 kV, anode current of 34 mA, measurement step of 0.02° 2θ and measurement range from 5° to 65° 2θ. Not oriented samples were prepared according to the procedure recommended for rocks with a high percentage of clay minerals [31]. The quantitative mineral composition of rocks was calculated by the Rietveld method [32] using the SIROQUANT program.

Oxygen and carbon isotopic determinations were performed for sixteen calcite and dolomite samples. Analyses were conducted in Germany, in GeoZentrum Nordbayern at the Friedrich-Alexander University Erlangen-Nürnberg. Carbonate powders were reacted with 100% phosphoric acid at 70 °C using a Gasbench II connected to a ThermoFisher Delta V Plus mass spectrometer. All values are reported per mille relative to VPDB [33]. Reproducibility and accuracy were monitored by replicate analysis of laboratory standards calibrated by assigning a $\delta^{13}C$ of +1.95‰ to NBS19 and −47.3‰ to IAEACO9 and a $\delta^{18}O$ of −2.20‰ to NBS19 and −23.2‰ to NBS18. Reproducibility for $\delta^{13}C$ and $\delta^{18}O$ was ±0.03 and ±0.06 (1 std. dev., respectively). Oxygen isotope values of dolomite were corrected using the phosphoric acid fractionation factors given by [34,35].

Fluid inclusion analyses have been performed in forty two-sided-polished sections according to the step-wise procedure described by [36]. Fluid inclusions were analyzed using a Nikon Linkam freezing-heating stage. Observations were conducted employing a polarizing microscope both in transmitted and reflected lights (UV). Microthermometric analyses were calibrated against melting temperatures of pure chemicals and phase transitions in synthetic fluid inclusions (Synflinc standards, [37]). The uncertainty limits of freezing-heating modes are 0.2 °C below −100 °C, 0.1 °C between −100 °C and +100 °C and 1 °C above 100 °C until the equipment's temperature threshold. FI petrography was carried out according to instructions given by [15,17,19].

Studies on the character of inclusions were conducted using a Nikon Eclipse microscope with a fluorescent device. Apart from the ''inclusion petrography'' (compare: [38]), the inclusions were analyzed in ultraviolet and blue lights. The fluorescence of hydro-

carbons was induced by ultraviolet reflected light in wafers prepared for fluid inclusion microthermometric studies. The long-wavelength light (368 nm) was provided by the 1200 W mercury lamp and a set of filters.

Fluid inclusion analyses were performed in carbonates and quartz. For carbonate types of cement, heating was conducted prior to freezing, as suggested by [19]. Calculations of microthermometric results were carried out using the combined FLUIDS package [39] and the simple FLINCOR program [40], which comprises less complicated chemical systems. Although the FLINCOR program has at present lesser importance because of the lack of compatibility with newer computer versions [41], it enables the first approximation of characteristics of fluids that fill the inclusions. The interpretation of microthermometric results (salinity based on T_m values) was also performed applying tables by [42].

Raman analyses were performed on four samples from two boreholes. The measurements were conducted using Thermo Scientific DXR™ equipment with an Nd-YAG laser (wave length of 532 nm). Details of measurements are described by [43]. The laser strength was 1–2 mW in the case of the organic matter and 5 mW for fluid and solid inclusions.

4. Results

4.1. Petrographic Characteristics

The Carboniferous sediments are represented by sandstones, mudstones and claystones.

Sandstones are mostly represented by sublithic, lithic and subarkosic wackes, with lesser arenites and locally quartz arenites (Figure 2A–H). The subarkosic variety is predominant in the Objezierze IG 1 borehole. Quartz arenites are present in the top part of the Katarzynin 2 borehole. Because of the high content of volcanic material, some sandstones are interpreted as volcanoclastic (the Katarzynin 2 borehole). The rocks are very fine- to fine-grained, only locally medium- or coarse-grained. The detrital grains of sandstones are poorly sorted and range from sub-rounded to very angular. Their contacts are mainly straight and pointed. The sandstones display a psammitic texture and generally unoriented structure, and in some cases, they are oriented and underlined by mica flakes and clay minerals, rarely also by detrital grains and laminae of the organic matter (e.g., the Zakrzyn IG 1 borehole).

Mono- and polycrystalline quartz and the quartz of volcanic origin (very angular shape, corrosion bays) occur in the studied rocks. Potassium feldspars and plagioclases are also present (Table 1, Figure 2E–H). Potassium feldspars contain on average: 64.9 wt. % SiO_2, 18.7 wt. % Al_2O_3, 15.6 wt. % K_2O, 0.9 wt. % Na_2O and 0.1 wt. % TiO_2, while plagioclases (albite): 67.6 wt. % SiO_2, 20.4 wt. % Al_2O_3, 0.2 wt. % K_2O, 10.8 wt. % Na_2O, 0.7 wt. % CaO, 0.2 wt. % FeO and 0.1 wt. % MnO. The results of argilitization, carbonatization, albitization, chloritization and hematitization are seen in the feldspar grains. The feldspar grains have undergone a weak dissolution. Lithoclasts are the most important component of the sandstone fabric. They are represented by volcanic rocks (mainly felsic, rhyolitic, and to a lesser extent, those of an intermediate or alkaline character) (Figure 2C,D), fragments of volcanic glass, and, less frequently, by magmatic (granitoids) and metamorphic rocks (quartz-mica and quartz schists) and siliceous rocks as well. In the Katarzynin 2 borehole (depth 2501.1 m), carbonatic rocks (limestones with bioclasts) were observed. Lithoclasts are partly replaced by carbonates and hematite, being argilitized and chloritized. Micas—muscovite and biotite and chlorites occur in high amounts. Mica flakes are strongly undulated due to mechanical compaction. Micas are locally altered into phosphates or replaced by carbonates, hematite and pyrite. Zircon, apatite and rutile are accessory. Organic matter is present.

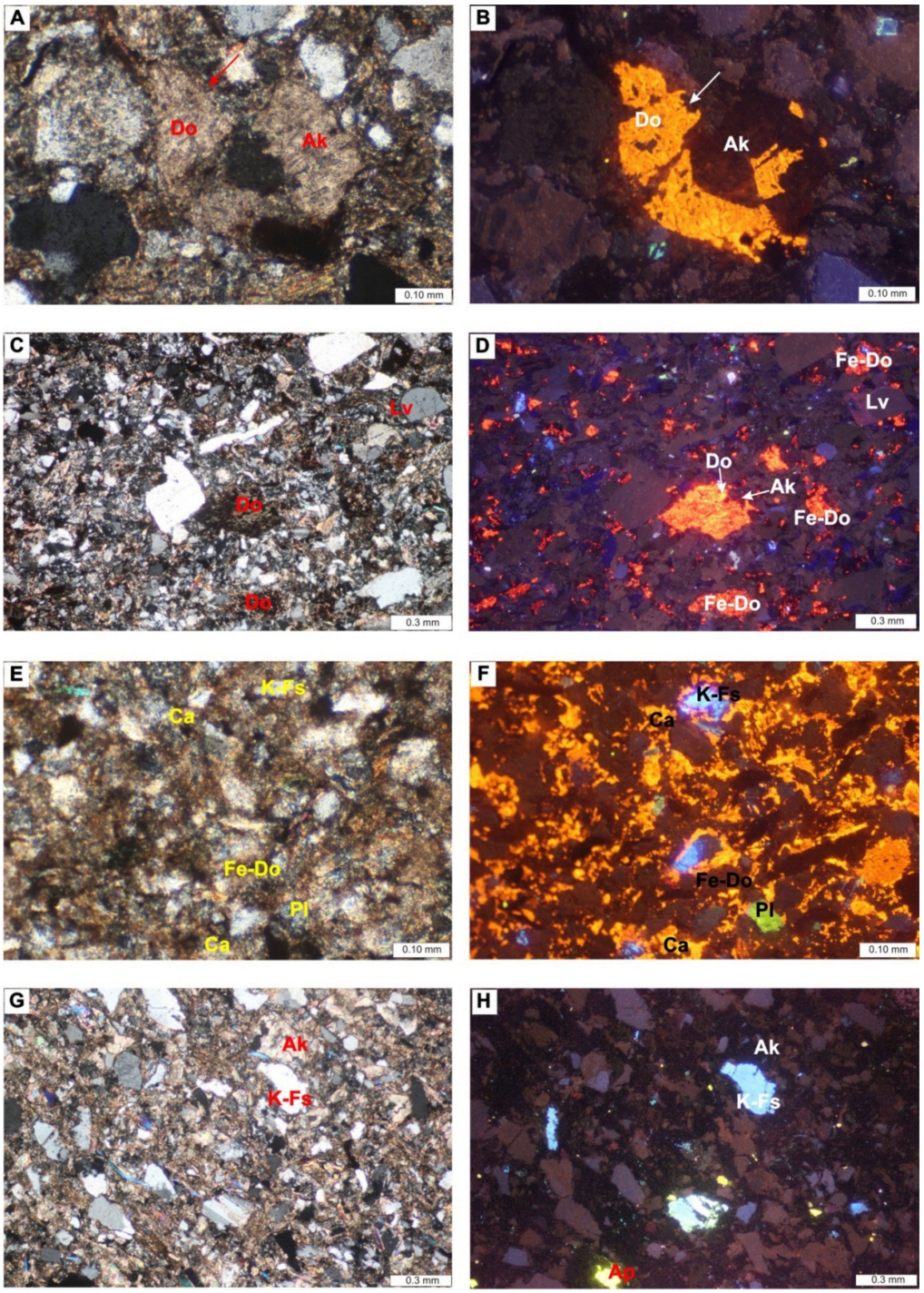

Figure 2. Photomicrographs of sandstones by a polarizing microscope (PL) and cathodoluminesence (CL). (**A**) A fragment of subarkosic wacke; dolomite (Do) and ankerite (Ak); ankerite replaces dolomite (arrow); Kalisz IG 1 borehole, depth of 3369.8 m, PL-crossed polars. (**B**) A CL image of the rock from Figure A; Dolomite (Do) displays orange luminescence, and ankerite (Ak) displays no luminescence; dolomite is replaced by ankerite (arrow). (**C**) A fragment of lithic wacke, which is a clast of acidic volcanic rock (Lv) and carbonates: dolomite (Do); Katarzynin 2, depth of 2374.1 m, PL-crossed polars. (**D**) A CL image of the rock from Figure C; the clast of acidic volcanic rock (Lv) displays brown-red luminescence, Fe-dolomite (Fe-Do) luminesce is red, dolomite (Do) is yellow, and ankerite (Ak) displays no luminescence. (**E**) A fragment of subarkosic arenite-potassium feldspar (K-Fs), plagioclase (Pl) and carbonate: calcite (Ca), Fe-dolomite (Fe-Do); Objezierze IG 1 borehole, depth of 5082.0 m, PL-crossed polars. (**F**) A CL image of the rock from Figure E; potassium feldspar

(K-Fs) displays light blue luminescence, plagioclase (Pl) is green and dark blue, calcite (Ca) luminesce is yellow-orange, and Fe-dolomite (Fe-Do) has no luminescence. (**G**) A fragment of sublithic arenite-potassium feldspar grains (K-Fs) and ankerite cement (Ak); Zakrzyn IG 1 borehole, depth of 4905.4 m; PL-crossed polars. (**H**) A CL image of the rock from Figure G; potassium feldspar (K-Fs) displays light blue luminescence, apatite (Ap) yellow, and ankerite (Ak) has no luminescence.

Table 1. Results of microprobe chemical analysis of feldspars.

Borehole	Depth (m)	Rock Type	Analytical Point	SiO_2	Al_2O_3	K_2O	Na_2O	CaO	FeO	TiO_2	MnO	Feldspar Type
Katarzynin 2	2588.1	sublithic wacke	1	63.98	22.00	0.33	9.35	2.68	0.08	0.08	0.02	Albite
			2	65.46	18.95	14.41	1.54	0.00	0.05	0.08	0.00	K-feldspar
			3	64.48	21.74	0.54	10.22	0.76	0.20	0.01	0.09	Albite
	2591.8	sublithic wacke	1	68.10	20.87	0.43	10.87	0.43	0.59	0.03	0.06	Albite
Objezierze IG 1	5083.9	subarkosic wacke	1	66.66	21.56	0.24	9.10	2.26	0.00	0.03	0.00	Albite
			2	69.18	19.68	0.06	10.62	0.36	0.00	0.00	0.00	Albite
			3	68.27	20.50	0.56	10.58	0.47	0.00	0.00	0.00	Albite
	5085.7	subarkosic wacke	1	63.49	18.89	16.22	0.43	0.00	0.00	0.12	0.13	K-feldspar
	5090.0	subarkosic arenite	1	65.35	18.43	16.02	0.99	0.01	0.00	0.00	0.00	K-feldspar
			2	69.55	19.49	0.00	12.14	0.00	0.08	0.00	0.00	Albite
			3	65.39	18.42	16.57	0.46	0.12	0.00	0.00	0.00	K-feldspar
Zakrzyn IG 1	4599.1	sublithic wacke	1	66.86	21.49	0.12	9.87	1.44	0.17	0.00	0.16	Albite
			2	68.42	20.66	0.42	10.41	0.14	0.11	0.00	0.10	Albite
			3	68.54	19.92	0.08	12.35	0.00	0.20	0.00	0.10	Albite
			4	67.89	18.63	0.17	12.03	0.20	0.04	0.00	0.04	Albite
			5	67.90	19.12	0.02	12.11	0.04	0.00	0.00	0.00	Albite
	4721.7	sublithic wacke	1	69.41	19.09	0.21	10.34	0.04	0.95	0.09	0.12	Albite
			2	67.44	20.94	0.05	10.70	1.40	0.01	0.01	0.09	Albite

The cement of sandstones is differentiated. A clayey, clayey-siliceous and clayey-ferruginous matrix is the main cement component of the wackes. X-ray analysis showed the presence of illite and chlorite. In the SEM images, a microporosity between clay mineral flakes may be seen. Mixed-layered minerals illite/smectite of ~80 to >90% illite content and chlorites (Figure 3A) represent authigenic clay minerals. The illite flakes recrystallize and occur in forms transitional to muscovite. Fibrous illite (Figure 3B) and vermicular and blocky kaolinite (Figure 3C) are also observed in the pore space.

Dolomite, Fe-dolomite, ankerite, rare calcite and local minerals from the siderite-magnesite group (sideroplesite) (Figures 2A–H and 3D) are the main carbonatic cement components in the sandstones. Authigenic quartz in the form of irregular regeneration overgrowths covers the detrital grains (Figure 3E,F). Prismatic barite is sporadic (Figure 3G), primarily being in places overgrown by celestite. Hematite and pyrite are present.

Many sandstones are cut by veinlets filled with carbonate minerals (Fe-dolomite/ankerite), anhydrite and quartz (Figure 3H). Locally, open fissures can be observed as well.

Mudstones (mudstones and sandy mudstones) form interlayers with sandstones and claystones. They display pelitic-aleuritic-psammitic textures. They exhibit oriented structures (underlined by mica flakes, hematite and organic matter). The detrital material, sub-rounded and angular, is represented by quartz, feldspars (plagioclases and potassium feldspars) and lithoclasts. Felspar grains and lithoclasts are replaced by calcite, hematite or altered into clay minerals. Micas (muscovite and partly chloritized biotite), abundant laminae of organic matter and pyrite are also present. Apatite is an identified accessory.

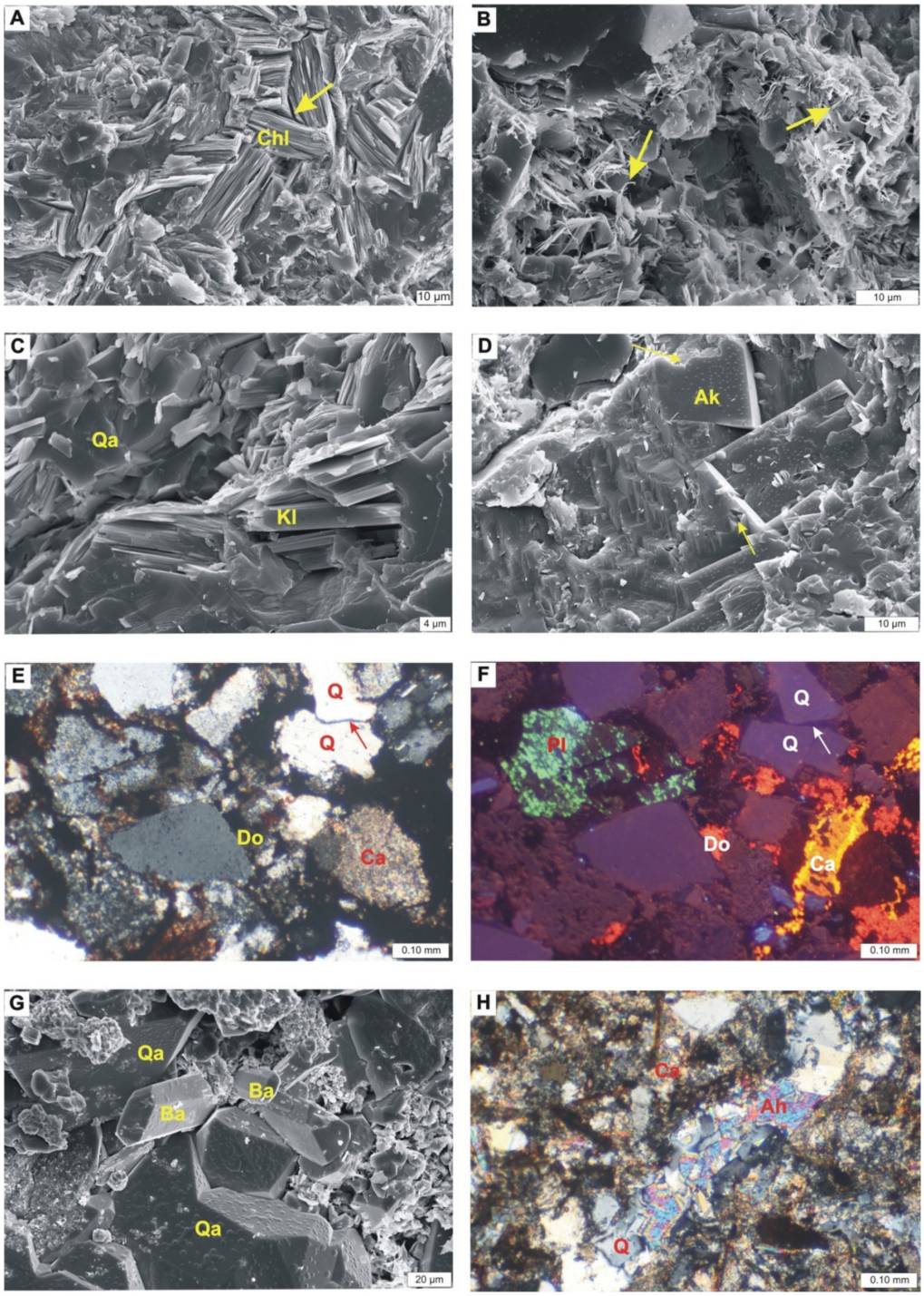

Figure 3. Photomicrographs of sandstones from a polarizing microscope (PL), cathodoluminesence (CL) and a scanning electron microscope (SEI). (**A**) Flakes of authigenic chlorite (Chl); distinct microporosity (arrow); Kalisz IG 1 borehole, depth of 3584.7 m, SEI image. (**B**) Fibrous illite in the pore space of volcanoclstic, lithic wacke; Katarzynin 2, depth of 2640.0 m, SEI image. (**C**) Authigenic kaolinite (Kl) with authigenic quartz (Qa) in subarkosic wackes; Objezierze IG 1 borehole; depth of 4964.8 m, SEI image. (**D**) Rhombohedra of ankerite (Ak); ankerite dissolution (arrows); SEI image; Kalisz IG 1 borehole, depth 3423.1 m. (**E**) A fragment of sublithic arenite-quartz (Q), plagioclase (Pl), cements: quartz (arrow) and carbonates: calcite (Ca) and dolomite (Do); Zakrzyn IG 1 borehole, depth of 4584.5 m; PL-crossed polars. (**F**) A CL image of the rock from Figure A; plagioclase (Pl) of blue-green luminescence, partly albitized (black-brown) and replaced by dolomite (red color), quartz

(Q) of brown-blueish luminescence, authigenic quartz (arrow) with no luminescence, yellow-orange calcite (Ca) and orange-red dolomite (Do). (**G**) Barite prisms (Ba) and authigenic quartz (Qa) in the intergranular space in quartz arenite; Katarzynin 2, depth of 2370.4 m, SEI image. (**H**) Veinlet filled with anhydrite (Ah), quartz (Q) and calcite cement (Ca) in sublithic wacke; Kalisz IG 1 borehole, depth of 3379.1 m, PL-crossed polars.

The detrital grains are surrounded by a clayey or clayey-ferrugineous groundmass. Illite and chlorites are identified as clay minerals and mixed-layered illite/smectite as well. Dolomite and ankerite, and less abundant calcite are the main carbonates.

Small veins filled with carbonates (ankerite, calcite) and anhydrite occur in the mudstones.

Claystones are dark grey rocks, many with parallel dark trails of organic matter, hematite and clay minerals. They display a pelitic-aleuritic texture. Quartz grains, feldspars with a plagioclase predominance over K-feldspar and micas occur as detrital components, as well as organic matter.

The clayey ground mass is built of illite and chlorites and mixed-layered illite/smectite minerals. Carbonates, such as calcite and Fe-dolomite, occur in low amounts.

The claystones are cut with veins that contain carbonates (dolomite and Fe/dolomite, calcite), quartz, anhydrite, kaolinite and bitumen.

4.2. Carbonate Minerals

The carbonate minerals in the studied rocks form cements or fill veinlets. Dolomite, Fe-dolomite and, less frequently, ankerite are the main carbonate minerals. Calcite occurs in low amounts (Table 2, Figures 2A–H, 3D and 4). Dolomite and Fe-dolomite contain: from 93.2 to 52.0 mole % $CaCO_3$ (in average 55.7 mole %), from 23.6 to 45.1 mole % $MgCO_3$ (in average 38.1% mol.), from 11.4 to 0.1 mole % $FeCO_3$ (in average 3.6 mole %) and from 6.5 to 1.2% mol. $MnCO_3$ (on average 2.4 mole %). The average chemical composition of ankerite is: 51.7 mole % $CaCO_3$, 22.6 mole % $MgCO_3$, 23.8% mol. $FeCO_3$ and 1.9% mol. $MnCO_3$. Calcite represents manganese-ferruginous varieties and comprises on average: 95.8 mole % $CaCO_3$, 1.1 mole % $MgCO_3$, 1.1 mole % $FeCO_3$ and 1.9 mole %$MnCO_3$. A mineral from the siderite-magnesite group (sideroplesite) was identified in samples from the Katarzynin 2 borehole (Figure 4).

Table 2. The results of the electron microprobe analysis of carbonates.

Borehole	Depth (m)	Rock Type	Analytical Point	Mg wt%	Ca wt%	Mn wt%	Fe wt%	$MgCO_3$ mole%	$CaCO_3$ mole%	$MnCO_3$ mole%	$FeCO_3$ mole%	Carbonate Type
Kalisz IG 1	3570.1	subarkosic arenite	1	11.80	22.28	0.94	1.80	40.2	54.2	1.9	3.6	Dolomite
			2	13.51	21.86	1.25	0.13	45.1	52.1	2.5	0.3	Dolomite
			3	12.53	22.54	1.29	0.30	42.4	54.4	2.6	0.6	Dolomite
			4	12.59	22.84	0.57	0.15	42.9	55.6	1.2	0.3	Dolomite
			5	6.55	20.57	0.64	10.96	23.3	52.3	1.4	23.1	Ankerite
	3598.0	muddy claystone	1	10.87	22.87	0.88	2.04	37.8	56.2	1.8	4.2	Fe-dolomite
			2	7.78	21.15	1.01	8.95	27.0	52.5	2.1	18.4	Ankerite
			3	11.31	22.84	1.10	0.39	39.7	57.2	2.3	0.8	Dolomite
Katarzynin 2	2374.1	lithic wacke	1	12.19	23.17	0.58	0.04	41.9	56.8	1.2	0.1	Dolomite
			2	2.72	0.85	0.33	41.38	9.7	2.2	0.7	87.4	sideroplesite
			3	5.54	21.49	1.04	12.77	19.0	52.8	2.2	26.0	Ankerite
			4	10.99	21.36	1.05	4.12	37.5	52.0	2.2	8.3	Fe-dolomite
			5	10.68	22.43	1.78	1.89	37.0	55.5	3.7	3.8	Fe-dolomite
Objezierze IG 1	5085.7	subarkosic wacke	2	0.20	36.96	0.84	0.40	0.7	96.6	1.8	0.9	Mn/Fe-calcite
	5090.0	subarkosic arenite	1	0.30	38.22	0.94	0.57	1.1	95.8	2.0	1.2	Mn/Fe-calcite
			2	0.64	37.91	1.27	1.12	2.2	92.9	2.6	2.3	Mn/Fe-calcite
			3	8.51	23.49	3.11	2.56	29.7	58.5	6.5	5.3	Fe-dolomite
			4	0.21	38.33	1.19	0.10	0.7	96.5	2.5	0.2	Mn-calcite
			5	6.74	25.23	2.67	3.68	23.6	63.2	5.6	7.6	Fe-dolomite
Zakrzyn IG 1	4560.2	sublithic arenite	1	10.52	21.93	0.70	3.96	36.3	54.1	1.4	8.1	Fe-dolomite
			2	12.71	21.20	0.66	0.36	44.7	53.2	1.4	0.8	Dolomite
			3	12.53	22.08	0.96	0.44	43.0	54.1	2.0	0.9	Dolomite
			4	9.42	21.60	0.81	5.52	32.9	54.0	1.7	11.4	Fe-dolomite
	4564.3	sublithic wacke	1	0.22	38.62	0.37	0.50	0.8	97.4	0.8	1.0	Fe/Mn-calcite
			2	10.10	23.07	1.29	2.83	36.2	59.0	2.8	2.1	Dolomite
			3	11.02	23.76	1.13	0.64	37.9	58.4	2.3	1.3	Dolomite
	4705.4	sublithic wacke	1	10.82	21.98	1.26	2.76	37.5	54.3	2.6	5.6	Fe-dolomite
			2	6.06	19.83	0.94	13.62	21.0	49.1	2.0	27.9	Ankerite

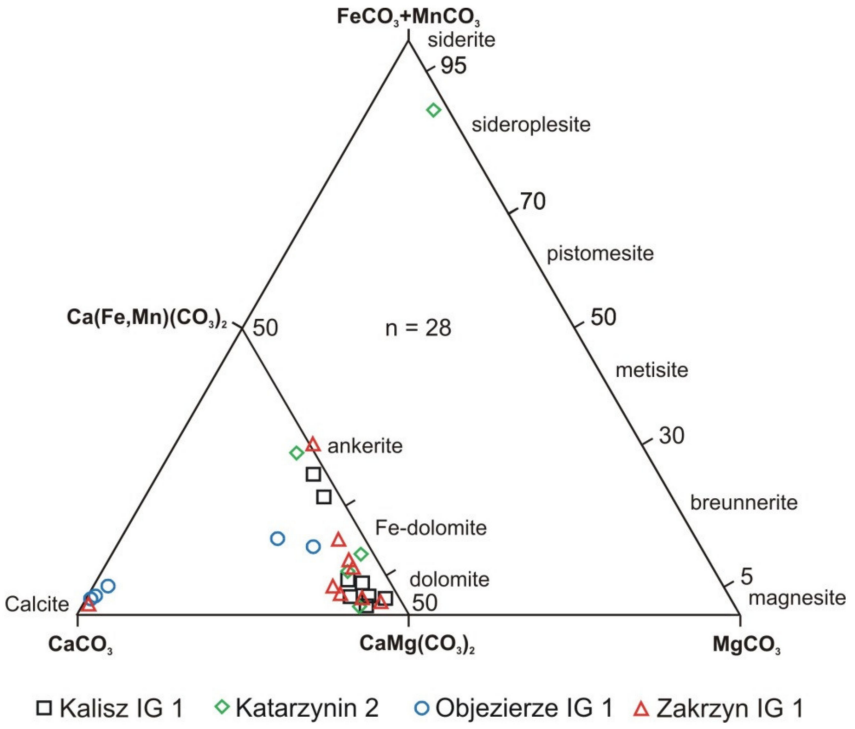

Figure 4. Ternary plot of the carbonates' chemical compositions at mole %; n—analysis number.

4.3. Isotope Analyses

The results of isotopic analyses of the selected samples are shown in the Table 3 and in Figure 5. Dolomite, Fe-dolomite and ankerite were analyzed. Their exact separation was impossible. Since the dolomite and its ferruginous variety are dominant, in the further interpretation, it is assumed that the results correspond to dolomite-ankerite. In three samples, the measurements for calcite were obtained. The δ^{13}C V-PDB values for dolomite-ankerite change from −7.35 to 4.19‰, (average 1.13‰), while δ^{18}O V-PDB results are in the interval from −0.42‰ to −10.01‰, (average −4.01‰). The δ^{13}C VPDB results for calcite are from −8.68‰ to −4.96‰, while the δ^{18}O V-PDB values change from −15.18‰ to −14.38‰.

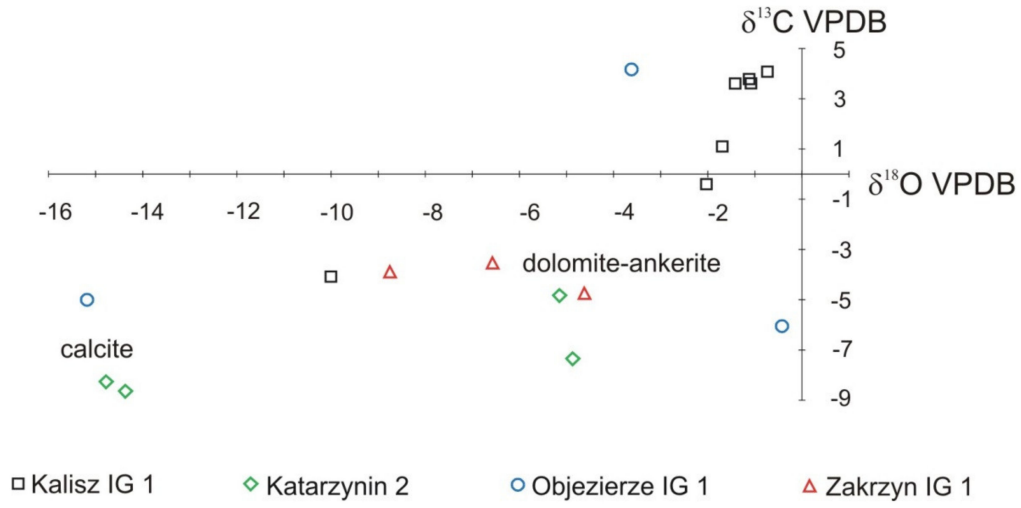

Figure 5. δ^{18}O‰ VPDB versus δ^{13}C‰ VPDB plot of carbonate minerals studied in four boreholes.

Table 3. Carbon and oxygen isotopic data.

Borehole	Depth (m)	Type of Carbonate Mineral	Delta 13 C ‰ VPDB	Delta 18 O ‰ VPDB
Kalisz IG 1	3368.80	Dolomite-Ankerite	4.07	−0.74
Kalisz IG 1	3369.80	Dolomite-Ankerite	3.59	−1.44
Kalisz IG 1	3379.10	Dolomite-Ankerite	3.75 3.61	−1.14 −1.08
Kalisz IG 1	3461.00	Dolomite-Ankerite	1.08	−1.70
Kalisz IG 1	3475.20	Fe-dolomite/Ankerite	−0.39	−2.03
Kalisz IG 1	3589.30	Dolomite-Ankerite	−4.05	−10.01
Katarzynin 2	2374.10	Dolomite-Ankerite	−4.84	−5.15
Katarzynin 2	2432.30	Calcite	−8.68	−14.378
Katarzynin 2	2588.45	Calcite	−8.28	−14.78
Katarzynin 2	2638.60	Dolomite-Ankerite	−7.35	−4.87
Objezierze IG 1	4895.70	Dolomite-Ankerite	−6.07	−0.42
Objezierze IG 1	4900.20	Dolomite-Ankerite	4.19	−3.62
Objezierze IG 1	5082.50	Calcite	−5.00	−15.18
Objezierze IG 1	5082.50	Calcite	−4.96	−15.17
Zakrzyn IG 1	4705.40	Dolomite-Ankerite	−4.78	−4.63
Zakrzyn IG 1	4872.20	Fe-dolomite/Ankerite	−3.90	−8.74
Zakrzyn IG 1	4905.40	Ankerite	−3.58	−6.57

4.4. Fluid Inclusion Petrography

Fluid inclusion studies concerned samples from three boreholes, such as: Katarzynin 2, Objezierze IG 1 and Zakrzyn IG 1.

Two main types of the pore and fracture filling are present: carbonate and quartz cements and carbonate veins (calcite, Fe-dolomite/ankerite).

The observed inclusions are rare and small (in general ~1–3 μm, some larger), presenting difficulty both in inclusion observation and microthermometry. The shape of inclusions is variable, with no preferred form. Some inclusions are oval, while others are more or less regular, and some are angular. Evidence of stretching and/or necking down is observed in some inclusions.

Fluid inclusions are either primary or secondary. They display either one phase or two phases. The liquid-to-vapor ratio (L:V) is generally differentiated, mostly with a predominance of the liquid. Occasionally, two different phases of L1 and L2 types (compare: ref. [44]) co-occur. A microscopic distinguishing of distinct assemblages of two-phase inclusions FIA (Fluid Inclusion Assemblage, see: [17,19]) is often impossible due to a low abundance of such inclusions. In some cases, entire assemblages of one-phase inclusions were observed.

4.5. Microscopic and Microthermometric Results

White carbonate veins occur in samples from the Carboniferous rocks in the Objezierze IG 1 borehole, where one-phase and two-phase inclusions are present (Figure 6A–D). In UV, these inclusions either do not fluoresce, or they display a faint dull blue fluorescence. In a few cases, a pale-yellow fluorescence of individuals or less common inclusion assemblages may be observed in a carbonate veinlet (Objezierze IG 1, depth of 4895.7 m; Figure 6A,B). In transmitted light, these inclusions of ~6 μm in size seem to be filled with a yellowish liquid. Freezing reveals the presence of "a bubble", i.e., a bi-phase character of inclusions.

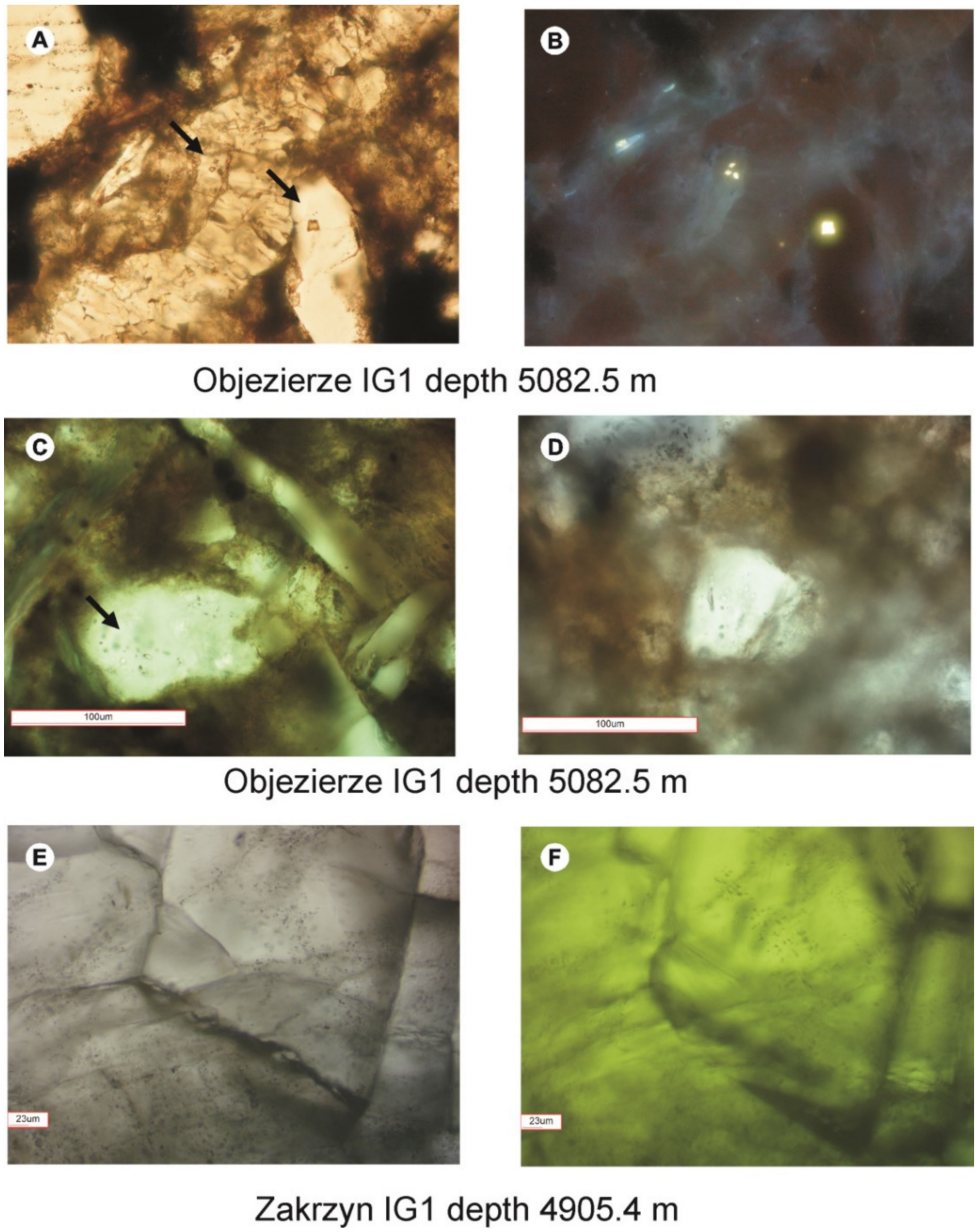

Figure 6. Fluid inclusions in different minerals and boreholes. (**A**,**B**) The fluorescent yellow fluid in inclusions in vein calcite. (**C**,**D**) Not fluorescent two-phase inclusions. Objezierze IG 1 borehole, depth of 5082.5 m. (**E**,**F**) Not fluorescent small inclusions in ankerite. Zakrzyn IG 1 borehole, depth of 4905.4 m. Images in transmitted (**A**,**C**–**E**) and reflected (**B**,**F**) lights.

Microthermometric results of the FI studies, both aqueous (AQFI) and hydrocarbon (HCFI) inclusions, are presented in Table 4. The measured values correspond to the following: T_h—homogenization temperature, T_e—eutectic temperature, T_m—ice melting temperature. Homogenization temperatures of two-phase inclusions in carbonates are generally high. They exceed 100 °C (up to 165 °C), while in quartz, they generally range between 120–200 °C with one higher value of 228 °C. In the sample from the depth of 4895.7 m, the eutectic temperature for dolomite-ankerite lies in the uniform interval between (−32) and (−38) °C. T_m is equal to −9.2 °C, which corresponds to a medium salinity of about 13 wt. %. NaCl eq. ([42]).

Table 4. Characteristics of fluids in fluid inclusions in the Objezierze IG 1 and Zakrzyn IG 1 boreholes *.

Sample	Microthermometry(°C)			Salinity (Weight % NaCl eq.)	Fluid Density (g/cm^3)	Type of Fluid	Remarks
Objezierze IG 1 Depth 4895.7 m	T_h	T_e	T_m				
AQFI	228		−7.5	11.10	0.926	Brine	Figure 6C,D
Quartz	200		−3.0	4.86	0.906		
	120		−2.4	3.96	0.972		
Dolomite-ankerite	90	−36.0	−9.2				Figure 6A,B
	104	−32.0		13.078	0.972		
Objezierze IG 1 Depth 5082.5 m							
AQFI	165	−44.3	−9.9	13.839	1.005		
	158	−44.3	−9.9	13.078			
Calcite	90	−36.0	−9.2		1.058	Brine	
	104	−42.0					
Quartz	120		−2.4	3.916	0.972		
Zakrzyn IG 1 Depth 4905. 4 m							
	76.9	−36	−5.0	7.82	1.027	Brine	Primary FI
AQFI	134.5	−44	−2.8	4.55	0.965		Secondary FI
Ankerite	115	−44	−2.8	11.82	0.965		
	160		−8.1				
HCFI		−88				CH_4	

* Calculations according to [40,42]. Based on [45]. Explanations: T_h—homogenization temperature; T_e—eutectic temperature; T_m—ice melting temperature.

In the sample from the depth of 5082.5 m, fluid inclusions were studied in carbonates and quartz. In the quartz overgrowth, a value T_m of −2.4 °C is obtained upon heating after a freezing run, which corresponds to a low salinity of the fluid trapped in this inclusion. The homogenization temperature of this inclusion was 120 °C. According to re-calculations of the experimental results using the FLINCOR program [40], in the chemical system of H_2O-NaCl, fluid salinity was estimated to be 3.9 weight % NaCl eq., which corresponds to a fluid density of ~0.972 g/cm^3 and a NaCl mole percentage of 0.021. The homogenization of aqueous inclusions trapped in the calcite occurred between 90 °C and 165 °C, with ice melting temperatures between −9.2°C and −9.9 °C (Table 4).

In the Zakrzyn IG 1 borehole, fluid inclusions were observed in the carbonates, which occur as veinlets filling the fissures (Figure 6E,F). Primary and secondary inclusions were observed in ankerite (Table 4, Figure 6E,F). Inclusions did not display fluorescence. The primary individuals with faint contours lie along the crystallographic directions. They are two-phase, liquid-gas, with the bubble smaller than 5% of the inclusion volume. In the sample from the depth 4905.4 m, primary inclusions in ankerite homogenize to liquid in temperatures between 76.9 °C and 134.5 °C (Table 4, Figure 6E,F; [45]). Ice melting temperature varies between −2.8 °C and −5.0 °C for primary inclusions. T_e values were measured in the interval from −44 °C to −36 °C. T_m changes suggest a low salinity of the fluid from ~7.8 wt. % to 0.2 wt. % NaCl eq. The secondary inclusions are well seen. They differ from the background, displaying an angular or rectangular habit. At room temperature, their "bubbles" comprise about 10% of the inclusion volume. A small unidentified solid phase is also possible. The T_h values of these inclusions lie between 147 °C and 165 °C. In Table 4, the FIA results of T_h = 160 °C and T_m = −8.1 °C correspond to these secondary inclusions. The homogenization of one-phase FIAs heated after deep freezing occurred at T_h = −88 °C.

The Carboniferous rocks in the Katarzynin 2 borehole were studied in the depth interval of 2432.3–2638.6 m. The carbonate minerals: calcite and Fe-dolomite/ankerite fill veinlets in the rocks. FI in calcite from the Katarzynin 2 borehole (depth of 2510.6 m) are two-phase and mono-phase (Figure 7). Their size falls to the interval of 3–6 µm. They are

AQFI and do not display a fluorescence excitation. Detailed results of microthermometric analyses are presented in Table 5. The T_h values are from 156–163 °C. T_m changes from −2.6 °C to almost 0 °C. The one phase inclusions display homogenization at −92.6 °C. The characteristics of inclusions from the sample from the depth of 2588.45 m are similar, although the homogenization temperature is much higher, reaching 233 °C.

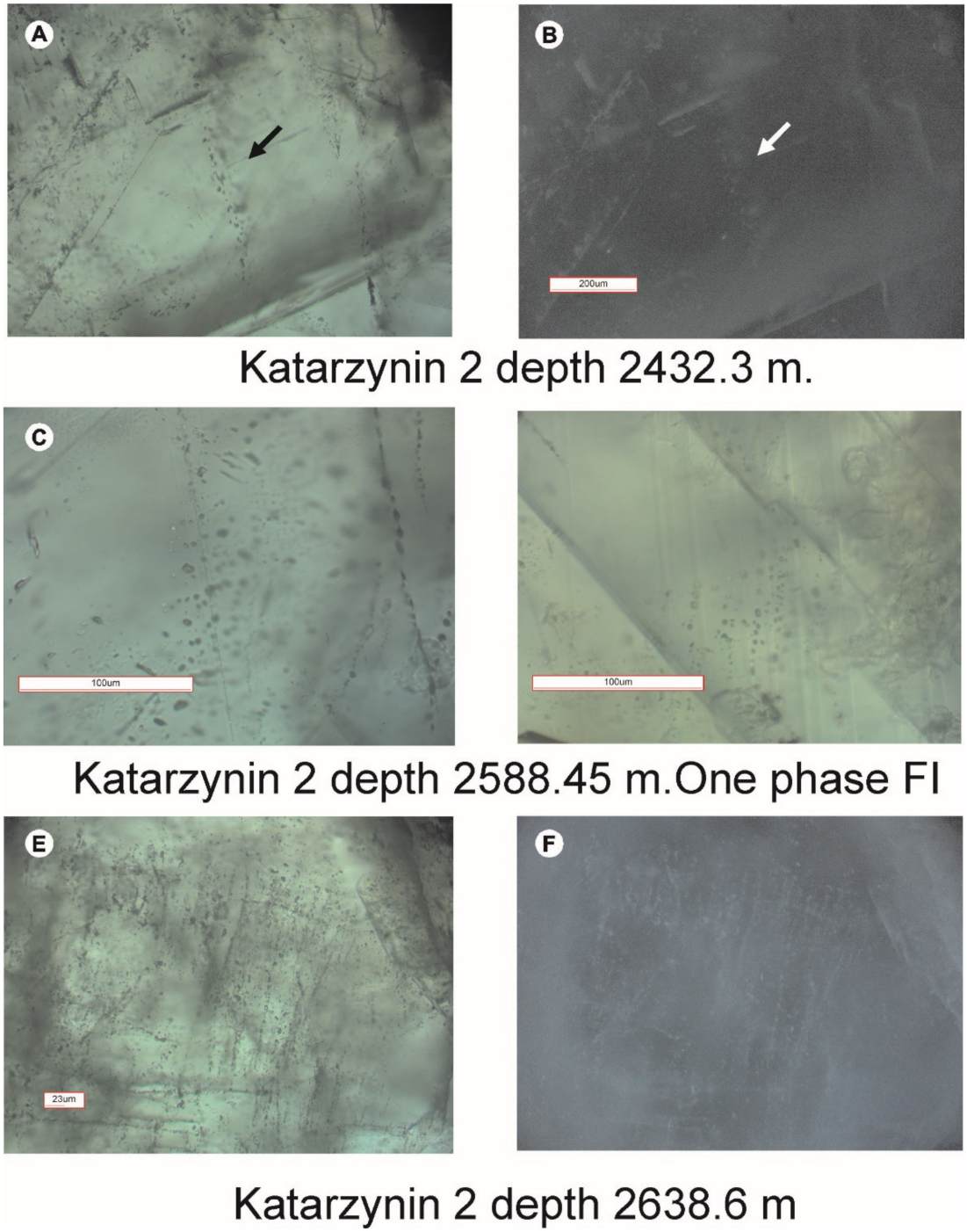

Figure 7. Fluid inclusions in carbonates in the Katarzynin 2 borehole section. Inclusions exhibit no fluorescence. Arrows point to the same objects as in photomicrographs. Polarized light, one polarizer (**A**,**C**–**E**); UV image (**B**,**F**).

Table 5. Characteristics of fluid inclusions in the Katarzynin 2 borehole.

Microthermometry					
Sample/ Inclusion Size	**Depth/ FI Character**	**T_h (°C)**	**T_e (°C)**	**T_m/T_c (°C)**	**Remarks**
Katarzynin 2	Depth 2432.3 m				Figure 7A,B; Raman analysis
Katarzynin 2 calcite	Depth 2510.6 m				
5 µm	Monophase rhombohedral elongated	−92.6			
3–6 µm	Two-phase rounded	156–163	−21	−2.6 to −0.1	
Katarzynin 2 calcite	Depth 2588.45 m				Figure 7C,D
2 µm	Monophase elongated	−96.6 +23.2			
2–3 µm	Two-phase angular	233	−44.3 to −38.0	−9.9 to −6.5/+2.2	
Katarzynin 2 Fe-dolomite/ankerite	Depth 2638.6 m				Figure 7E,F; Raman analysis
2–5 µm	Monophase elongated Oval	−101			
2 µm	Two-phase irregular	113	−33.0	−5.8/+1.5	

Explanations: T_h—homogenization temperature; T_e—eutectic temperature; T_m—ice melting temperature; T_c—clathrate melting temperature.

In detail, two-phase inclusions in calcite at the depth of 2588.45 m are smaller (2–3 µm) and filled with a brine, locally with an admixture of unidentified gas. T_h of the inclusions is very high and lies in the interval of 207−233 °C; T_e is between −48.8 °C and −38 °C, while T_m values were measured from −9.9 °C to −6.5 °C (Table 5).

As previously mentioned, mono-phase inclusions were observed in the samples from the Katarzynin 2 borehole. Abundant one-phase inclusions were present within crystals of Fe-dolomite/ankerite at the depth of 2638.6 m. The inclusions occurred in linear, oriented or random assemblages. In some cases, the co-occurrence of two phases, L1 + L2, was observed. The inclusions are in distinct FIAs. Their shape is close to oval or oval. They do not display fluorescence or are dull blue. One-phase inclusions homogenize at T_h = −101 °C, while the brine FIAs contain gas admixture and homogenize at T_h = 113 °C; T_e equals to −33 °C; T_m corresponds to −5.8 °C (Tables 5 and 6).

Table 6. Interpretation of the microthermometry results for the primary fluid inclusions in calcite and Fe-dolomite/ankerite.

Microthermometry							
Borehole Depth	**Mineral**	**T_h (°C)**	**T_e (°C)**	**T_m/T_c (°C)**	**Fluid Salinity (wt. % NaCl eq.)**	**Fluid Density (g/cm^3)**	**Remarks**
Katarzynin 2 2510.6 m	calcite	−92.6 156–163	−21	−2.6	4.232	0.274 0.938	CH_4 Brine I
Katarzynin 2 2588. 45 m	calcite	−96.6 233	+23.2 −44.3 to –38	−9.9 to −6.5/+2.2	13.839 9.844	0.290 0.942–0.911	CH_4 CO_2 Brine II
Katarzynin 2 2638.6 m	Fe-dolomite/ ankerite	−101 113		−5.8	8.92	0.304 1.011	CH_4 Brine III
Zakrzyn IG 1 4905.4 m	Ankerite	134.4 −88	−44	−2.8	4.6	0.965 0.251	Brine CH_4

Explanations: T_h—homogenization temperature; T_e—eutectic temperature; T_m—ice melting temperature; T_c—clatrathe melting temperature.

4.6. Raman Analyses

The Raman analyses were only performed for samples from the Zakrzyn IG 1 (depth 4905.4 m) and the Katarzynin 2 boreholes (depth 2432.3 m, 2588.45 m and 2638.6 m—Raman: Kat5, Kat24 and Kat30, respectively).

In the Zakrzyn IG 1 borehole, the inclusions display sizes from a few to over 10 µm. The Raman spectra of FI did not show the presence of gas peaks. They distinctly point to the presence of solid inclusions, such as hematite and organic matter (Figure 8A,B, respectively).

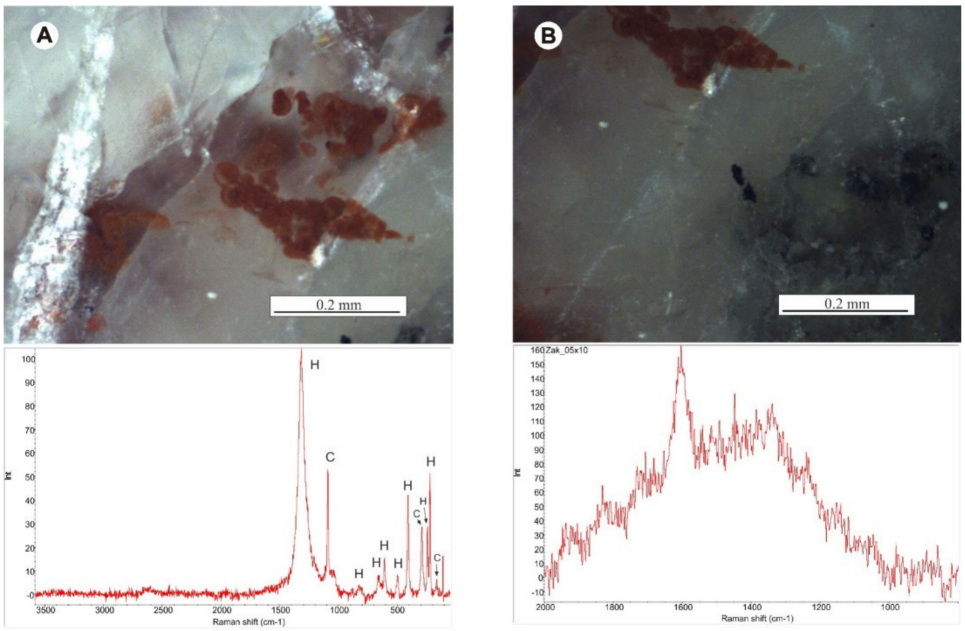

Figure 8. Photomicrographs and Raman spectra for solid inclusions of (**A**) hematite and (**B**) organic matter in the Zakrzyn IG 1 borehole (depth 4905.4 m).

In the Katarzynin 2 borehole, the organic matter (CM) in two studied samples from the depth of 2432.3 m and 2638.6 m, respectively, (Kat5, Kat30) occurs in the form of small accumulations. These inclusions are isometric to irregular. The analysis of the spectra

performed according to [46] results in temperatures of thermic alterations of about 164 °C (Kat5) and 197 °C (Kat30) (Table 7).

Table 7. Parameters of Raman spectra for organic matter accumulations*.

Sample no. and Statistic Parameters	FWHM D4 (cm^{-1})	FWHM D1 (cm^{-1})	FWHM D3 (cm^{-1})	FWHM G (cm^{-1})	Temperature 1 (°C)	Temperature 2 (°C)
			Katarzynin 2 Depth 2432.3 m			
Kat5_01 × 50	143.67	143.05	143.05	56.96	170.44	148.81
Kat5_02 × 50	139.42	151.82	151.82	56.36	151.58	152.87
Kat5_03 × 50	139.06	152.93	152.93	55.92	149.19	155.83
Kat5_04 × 50	148.42	140.94	140.94	57.1	174.98	147.86
Kat5_05 × 50	158.51	137.9	137.9	53.08	181.52	175.11
Mean	146.35	145.9	145.9	55.62	164.32	157.92
Mediana	143.92	146.38	146.38	56.14	163.28	154.35
SD	9.19	7.6	7.6	1.76	16.34	11.93
CV [%]	6.28	5.21	5.21	3.16	9.94	7.55
			Katarzynin 2 Depth 2638.6 m			
Kat30_01 × 50	119.54	141.08	190.88	50.27	174.67	194.18
Kat30_02 × 50	117.44	134	185.27	49.37	189.89	200.3
Kat30_03 × 50	117.6	135.11	184.8	48.79	187.51	204.17
Kat30_04 × 50	106.54	142.41	174.16	49.32	171.83	200.59
Kat30_05 × 50	114.07	135.77	255	49.45	186.09	199.73
Kat30_06 × 50	198.21	159.46	185.13	57.02	135.16	148.43
Kat30_06 × 50a	195.36	167.65	162.9	56.98	117.55	148.65
Kat30_07 × 50	113.2	131.41	303.44	49.27	195.46	200.96
Kat30_09 × 50	145.93	119.13	313.74	52.59	221.87	178.42
Kat30_10 × 50	129.31	123.04	304.38	43.26	213.46	241.69
Kat30_14 × 100	80.5	116.7	262.68	32.82	227.09	312.47
Kat30_19 × 100	108.31	101.87	237.03	29.5	258.97	335
Kat30_21 × 100	72.25	127.34	283.23	33.46	204.22	308.14
Kat30_23 × 100	107.7	93.98	232.71	35.12	275.93	296.91
Mean	12328	130.64	233.95	45.52	197.12	226.4
Mediana	115.75	132.71	234.87	49.3	192.68	200.77
SD	35.96	19.75	53.72	9.12	42.47	61.86
CV [%]	29.17	15.12	22.96	20.05	21.55	27.33

* Values of FWHM for the D4, D1, D3 and G bands, estimated temperature and basic statistical parameters. The position of bands: D4 (1250 cm^{-1}), D1 (1350 cm^{-1}), D3 (1500 cm^{-1}) and G (1580 cm^{-1}). SD—Standard deviation; CV—Coefficient of variation; Temp. 1—calculated from Equation 1 (according to [46]); Temp. 2—calculated from Equation 2 (according to [46]).

Fluid inclusions in the Kat5 and Kat24 samples occur in calcite and quartz together with some black solids. They are faint, however, in the reflected light images (Figure 9).

The Raman spectra in Kat 24 show some fluorescence that points to the presence of an undefined substance, probably organic compounds. In the sample Kat30, peaks of quartz and calcite were diagnosed. In a part of the spectrum, the methane peak (2917 cm^{-1}) is distinct, e.g., [47]. The distinct organic matter (CM) is also present, as seen in both the Raman spectra and photomicrographs (Figure 9C,D,F).

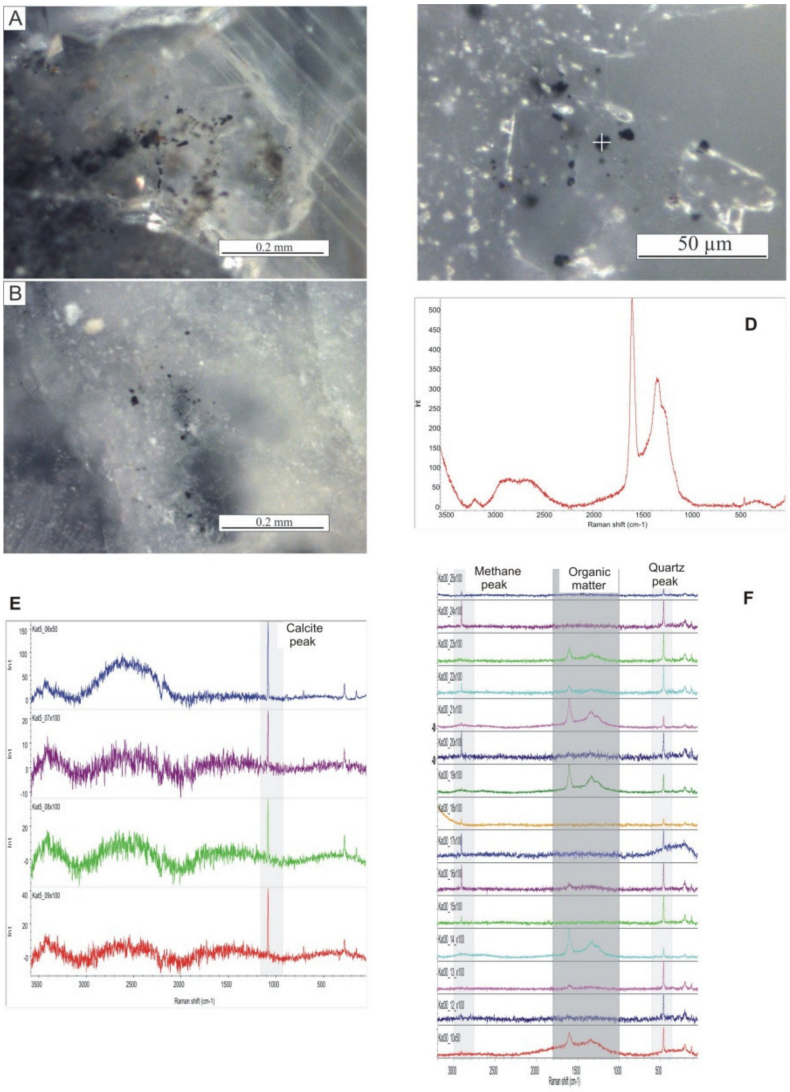

Figure 9. Photomicrographs and Raman spectra in the Katarzynin 2 borehole. (**A**–**C**) Fluid and solid inclusions in minerals. (**D**–**F**) Raman spectra showing calcite and quartz peaks together with organic matter.

5. Discussion

The studied samples of the Carboniferous rocks from the Fore-Sudetic Monocline presently occur at depths from ~2370 m at the top to ~2640 m at the bottom in the section of the Katarzynin 2 borehole, through the following depths in the Kalisz IG 1 borehole at ~3599 m, Zakrzyn IG 1 at ~ 4905 m and Objezierze IG 1 at ~5090 m.

5.1. Interpretation of Homogenization Temperatures of Fluid Inclusions and Trapping Conditions

The homogenization temperatures for inclusions are different between boreholes and vary with the type of mineral that either fills the veinlet or forms a cement in the rock.

According to [4], the veins are related to the Variscan orogeny, i.e., they are Carboniferous in age. Based on the results from [19,45,48] and the current research, the following types of inclusions occur: aqueous AQFI (two-phase) and hydrocarbon HCFI (HCFI 1—monophase and HCFI 2—two-phase). The AQFI in calcite and dolomite-ankerite from the Objezierze IG 1 borehole is filled with brine with salinity between 13.08 and 13.84 weight % NaCl eq. Occasional FIAs of yellow color and yellow fluorescence in the calcite vein are filled with oil of high maturity (compare: [49–51]).

Fluid inclusions in the Zakrzyn IG 1 borehole are also filled with a brine, locally with an admixture of methane and nitrogen. The presence of other components in the gas is not excluded, but the microthermometric evidence (just singular high eutectic temperature values) is too scare to enable more meaningful conclusions [45].

The presence of methane with a probable nitrogen component, and carbon dioxide as well, was also recognized in mono-phase inclusions (HCFI 1) in the Katarzynin 2 borehole in the Fe-dolomite/ankerite. Numerous assemblages of such individuals were observed, especially at the depth of 2638.6 m.

As for AQFI, at least three generations of AQFI of different characteristics occur in the Katarzynin 2 borehole [40,45,48]. The following fluids may be involved: I—a complex brine of, e.g., $CaCl_2$-MgCl-H_2O-NaCl [48], of salinity ~8.92 wt. % NaCl eq. and density 1.011 g/cm^3; II—a less complex brine of NaCl-H_2O composition [48], with salinity from 4 wt. % NaCl eq. to almost pure water, and density slightly below 1g/cm^3; III—a complex brine with Ca and Mg ions and medium salinity between 14 and 10 wt. % NaCl eq. (Tables 4–6; calculations according to [40–42]). This suggests several brine inflows and brine-methane front.

Some brine inclusions display a gas (methane) in the vapor phase. This suggests co-trapping of the brine and methane in the mineral. Based on that assumption, isochores for individual pairs of chemical systems of H_2O-NaCl and CH_4 were calculated (Table 8), and P-T conditions of a possible trapping were estimated using the method of crossing isochores (compare e.g., [49–51]). Isochores are presented in Figures 10 and 11. In the case of the Katarzynin 2 borehole, the results of the isochore calculations for a secondary inclusion are also presented (Table 8).

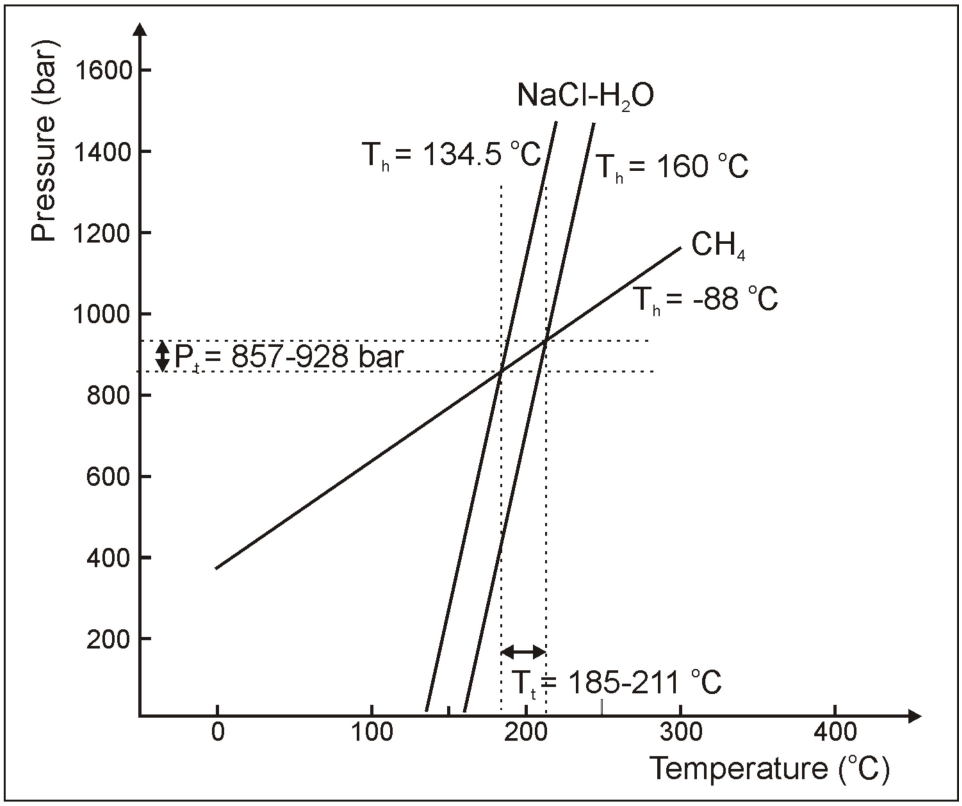

Figure 10. The estimation of P-T trapping conditions for AQFI (brine) and HCFI 1 (methane) in the Zakrzyn IG 1 borehole (depth 4905.4 m).

Table 8. Calculations of microthermometric results for selected groups of inclusions (based on FLINCOR [10]).

Sample/Depth (m)	**Chemical System**					
Zakrzyn IG 1/4905.4 m	**H_2O–Primary**		**NaCl inclusions**		**CH_4**	
Eqn of state	**Brown and Lamb ***		**Brown and Lamb**		**Holloway**	
Freezing point depression (°C)	−2.8		−8.1			
NaCl molality	0.815		2.294			
Mole fraction NaCl	0.014		0.040			
Weight per cent NaCl	4.55		11.821			
Vapor out temp. (°C)/ Homogenization (°C)	134.5		160		−88	
Bulk molar volume	19.27		19.73			
Critical point	416.1		482.3			
Density (g/cm^3)	0.965		0.994		0.251	
Isochore	Temperature (°C) pressure (bars)		Temperature (°C) pressure (bars)		Temperature (°C) pressure (bars)	
	150	280	200	710	150	766
	200	1168	250	1591	200	902
	250	2056	300	2472	250	1035
	300	2945			300	1166
Katarzynin 2/2510.6 m	**H_2O–Primary inclusion**		**NaCl Secondary inclusion**		**CH_4**	
Eqn of state	**Brown and Lamb**		**Brown and Lamb**		**Holloway**	
Freezing point depression (°C)	−2.6		−2.6			
NaCl molality	0.815		0.756			
Mole fraction NaCl	0.014		0.013			
Weight per cent NaCl	4.23		4.32			
Vapor out temp. (°C)/ Homogenization (°C)	156		163		−92.6	
Bulk molar volume	19.05		19.79			
Critical point	416.1		413.1			
Density (g/cm^3)	0.974		0.938		0.274	
Isochore	Temperature (°C) pressure (bars)		Temperature (°C) pressure (bars)		Temperature (°C) pressure (bars)	
	200	774	200	649	200	1078
	250	1648	250	1619	250	1236
	300	2389	300	2389	300	1392

* Not above 3 kb.

Based on the diagram presented above, it can be concluded that in the Zakrzyn IG 1 borehole (depth 4905.4 m), the co-trapping conditions of brine and gas could have been at a pressure of ~850–930 bars and temperatures in the interval of 185–210 °C for fluids that display homogenization in the interval T_h = 134.5–160 °C (AQFI in ankerite) and T_h = −88 °C (HCFI 1). This applies to pairs of brine/CH_4 inclusions (Table 8).

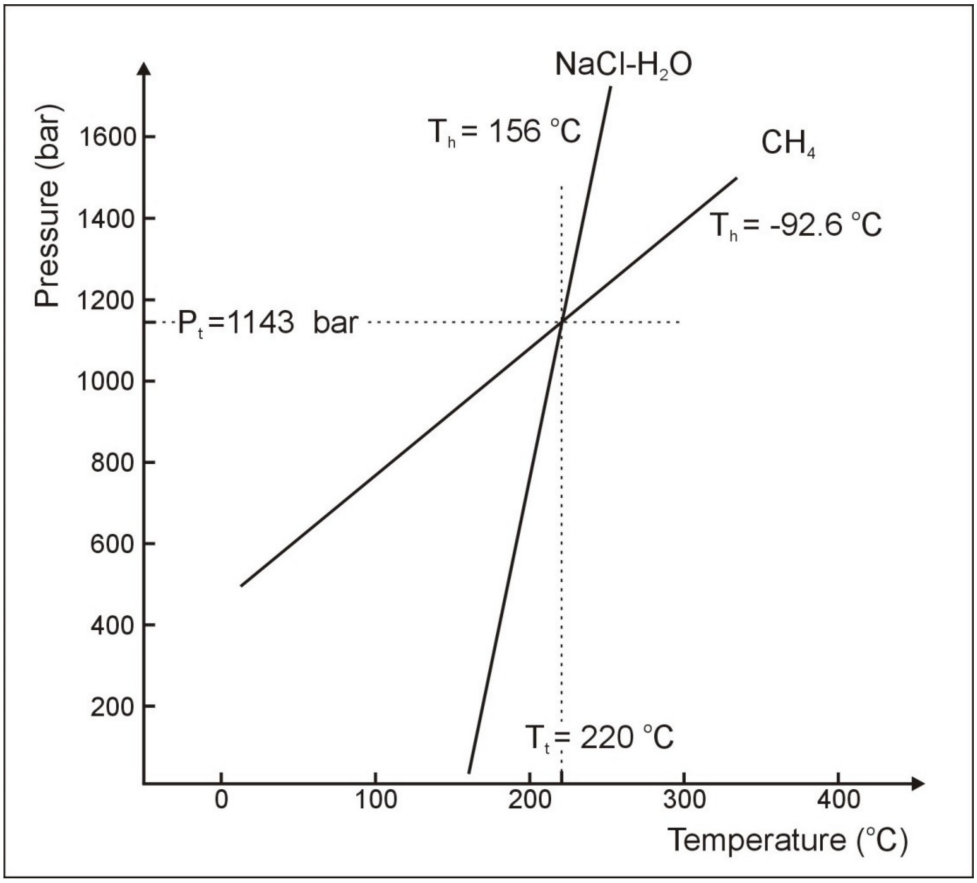

Figure 11. The estimation of P-T trapping conditions for AQFI (brine) and HCFI 1 (methane) in the Katarzynin 2 borehole (depth 2510.6 m).

Based on the diagram (Figure 11), it can be concluded that in the Katarzynin 2 borehole (depth 2510.6 m) for the aqueous inclusion that displays homogenization at T_h =156 °C in calcite and for methane (HCFI 1 of homogenization at T_h = −92.6 °C, Table 8), the co-trapping conditions for brine and gas could have been a pressure P_t = ~1143 bars and a temperature T_t = ~220 °C.

The fluid salinity varies in respect to the mineral filling the veins or forming the cement. It changes as follows: calcite 0–14 wt. % NaCl eq., Fe-dolomite/ankerite ~5 wt. % NaCl eq. and quartz ~4 wt. % NaCl eq. The density of fluids in AQFI is close to 1 g/cm^3 (Tables 4 and 6).

Observations of some groups of fluid inclusions, variable homogenization temperatures of two-phase individuals and unequal liquid-to-vapor ratios may suggest that some of values are not connected with the primary conditions of cement formation.

Most significant and important for interpretation are eutectic and ice melting temperatures. The values obtained imply a conclusion on the complex character of fluids migrating through the Carboniferous deposits [15,16,51].

5.2. Geochemical Environment of Crystallization of Carbonate Minerals

The δ^{13}C VPDB values for calcite in range of −8.68‰ to −4.96‰, and for Fe-dolomite/ankerite, they are between −7.35‰ and 4.19‰ (av. 1.13‰), which point to the mineral formation in the zone of a microbiological methanogenesis and thermal decarboxylation [52].

The Friedman-O'Neil formula [53] was used to estimate the δ^{18}O of pore water, from which the calcite crystallized (δ^{18}O VPDB from −15.18‰ to −14.38‰). Homogenization temperatures for calcite (Table 6) that correspond to the minimum estimate of calcite formation were used for the diagram (Figure 12A). The $\delta^{18}O_{SMOW}$ of pore waters, from

which calcite might have crystallized, are in the interval from ~−4‰ to ~4‰. The fluid salinity was as low as ~4 weight per cent NaCl eq.

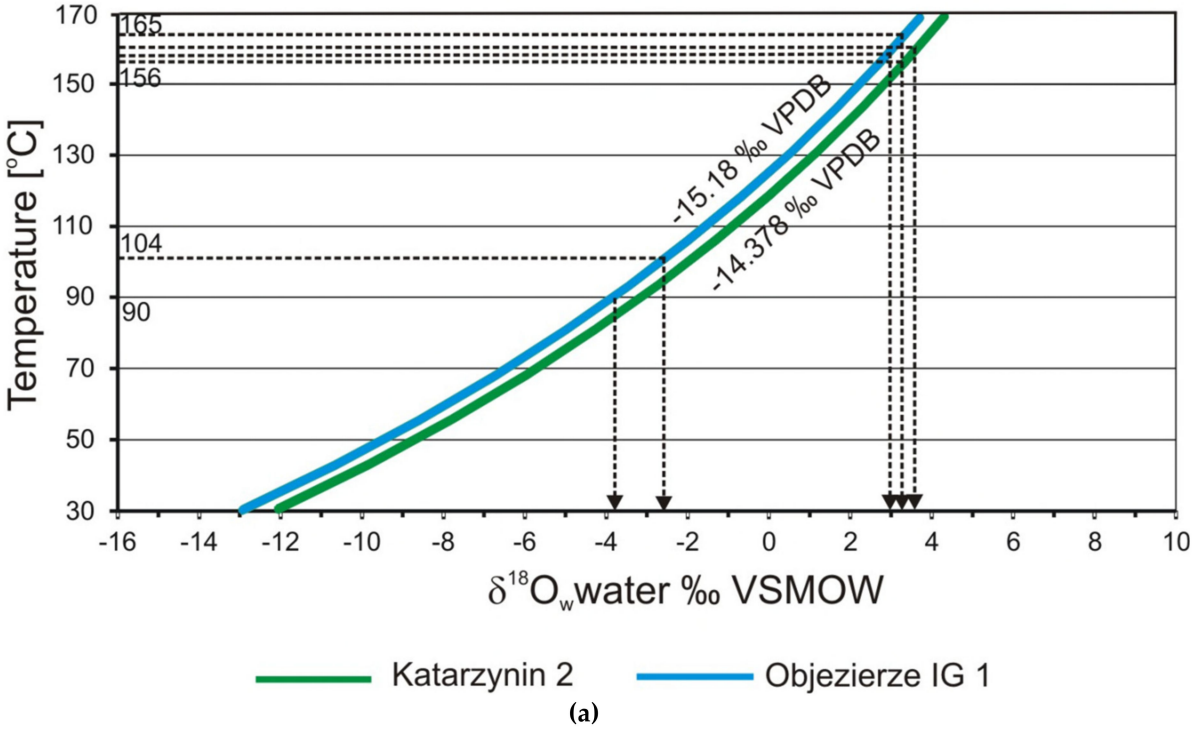

(a)

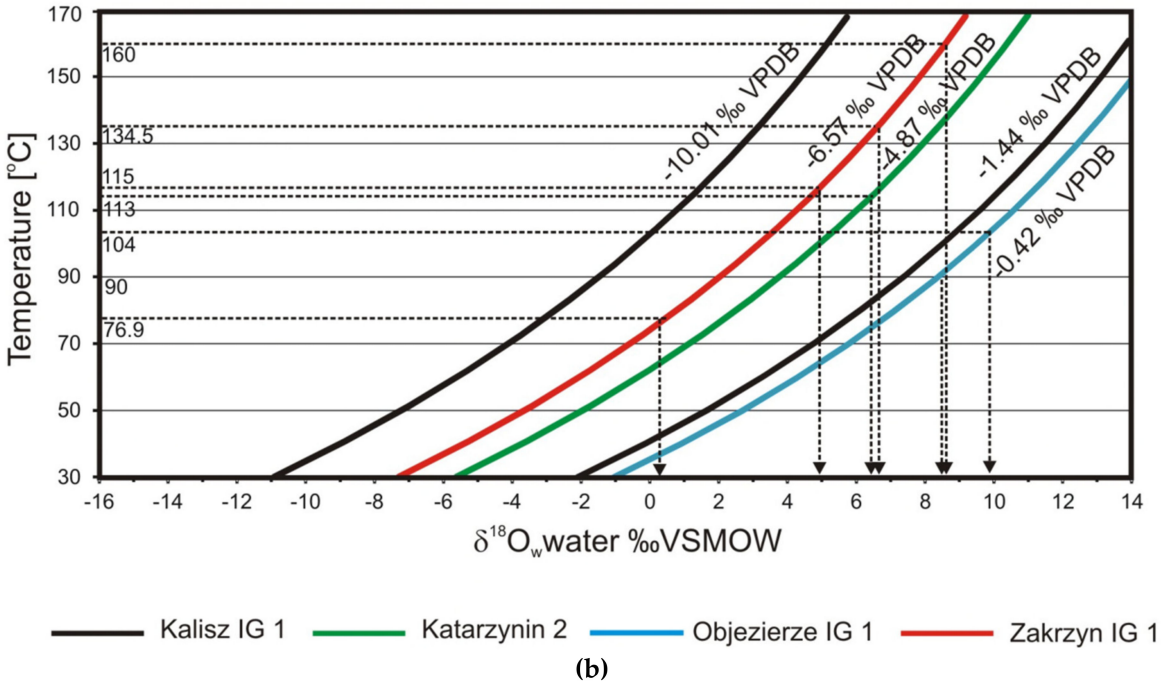

(b)

Figure 12. (**a**) Plot of $\delta^{18}O$ pore water versus temperature for calcite (after [53]); (**b**) Plot of $\delta^{18}O$ pore water versus temperature for Fe-dolomite/ankerite (after [54]).

The Dutton-Land formula [54] was used to estimate the $\delta^{18}O$ of pore water, from which the dolomite-ankerite crystallized ($\delta^{18}O$ VPDB from −0.42‰ to −10.01‰, −4.01‰ in average). Homogenization temperatures (Table 6) that correspond to the minimum estimate of mineral formation were used for the diagram (Figure 12B). The $\delta^{18}O_{SMOW}$ of pore waters, from which Fe-dolomite/ankerite might have crystallized at the later stage of

diagenesis, are in the interval from 0 to ~10‰ (most frequently >4‰). The fluid salinity was ~4.6 wt. % NaCl eq.

The analytical results obtained may confirm that at later diagenetic stages, calcite crystallized before Fe-dolomite/ankerite or at the same time. This is indicated by the $\delta^{18}O_{SMOW}$ values of pore waters responsible for the carbonate precipitation. In the Fe-dolomite/ankerite case, the pore waters are enriched in O^{18} isotope in comparison to the water from which the calcite crystallized. According to [55,56], the enrichment in O^{18} could have been caused by a water-rock reaction during burial. The inflow of marine waters cannot be also excluded, which is quite possible seeing many carbonate veins in the deposits.

5.3. Diagenetic Processes

The following diagenetic processes influenced the Carboniferous sediments in the study area: compaction, cementation, replacement, alteration and dissolution of the components, with a predominance of the two first processes [8]. In the diagenetic history of the deposits, these processes were manifested in the eo- and mesodiagenesis. This scheme is adopted from [57] and describes limestone diagenetic processes. According to [58], it is also applied in the clastic diagenesis.

The diagenetic sequence of the Carboniferous deposits in the Fore-Sudetic Monocline is presented in the diagram (Figure 13).

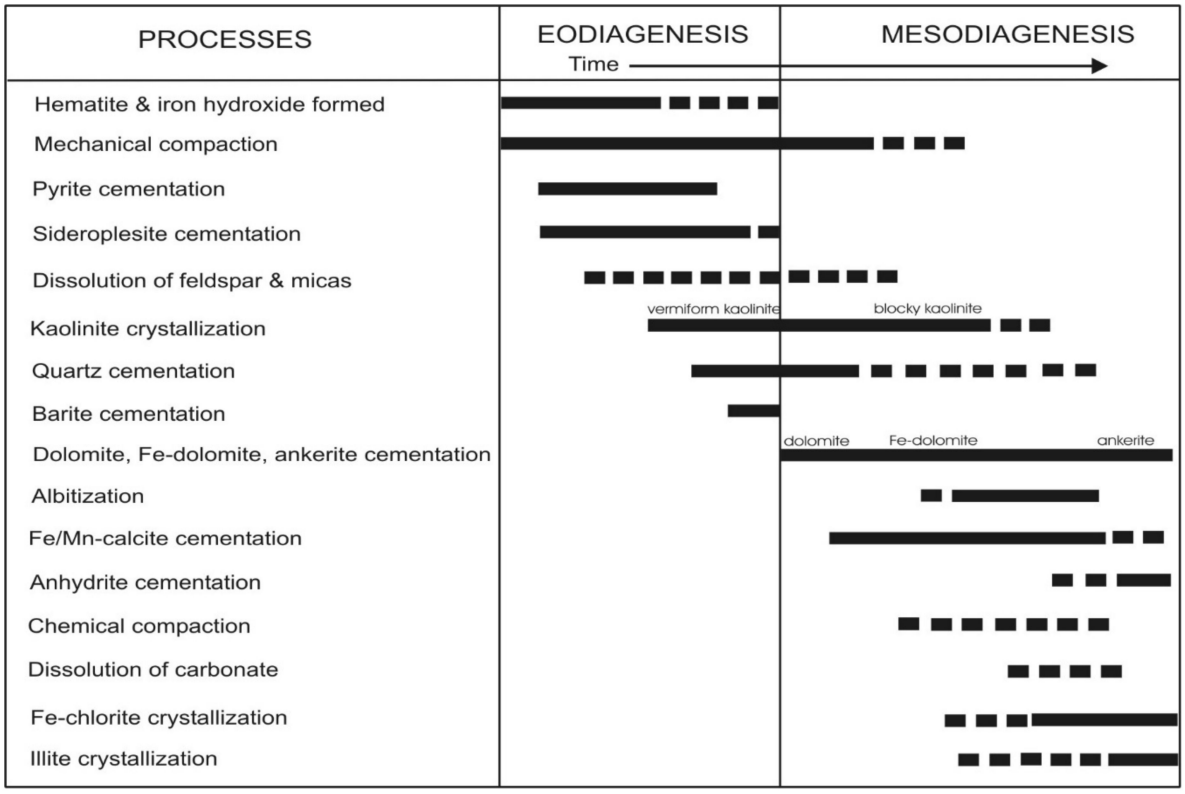

Figure 13. The synoptic paragenetic sequence of the Carboniferous sandstones.

5.3.1. Compaction

The mechanical compaction occurs at the beginning of the eodiagenesis. Its effects are seen as more compact packing of the detrital components. It also resulted in the undulation of mica flakes and plastic lithoclasts (volcanic rocks among others). Numerous fractures of detrital grains are seen, too. The mechanical compaction continues in the mesodiagenesis, being later followed by chemical compaction. Straight intergranular contacts are the results of that last process.

5.3.2. Cementation

Iron hydroxides and hematite formed in the oxidation conditions at the early stage of diagenesis. In general, the process of sediment enrichment in iron occurs at ~50 °C [59]. The pyrite crystallized in the eodiagenesis. It occurred in local conditions where the H_2S amount produced by sulfate-reducing bacteria exceeds the percentage of the reduced iron [60].

The vermicular kaolinite crystallized in acidic conditions at temperatures of ~25–50 °C in the eodiagenesis [61]. The blocky kaolinite, in its turn, formed at the later, mesodiagenetic stage, in the temperature interval of 50–80 °C [61]. Blocky dickite has not been confirmed. According to [62], the presence of dickite could be confirmed by XRD or infrared studies (not the present case), while its formation could be estimated for about 120 °C. The transformation of smectite to illite resulted in the illite/smectite mixed-layered minerals of about 80–90% illite. According to [63] a drastic increase of illite percentage in illite/smectite was observed at ~60–80 °C. The high illite content up to 90% in the mixed-layered illite/smectite mineral points to a temperature of ~160 °C, which influenced the rocks under discussion [64]. The fibrous illite is interpreted to be the authigenic mineral, which, in the diagenetic history, crystallizes the last. Bjørlykke estimates the temperature of fibrous illite crystallization as 120–140 °C [65].

Late diagenetic genesis also displays chlorites; the formation of which is referred to as the chloritization of kaolinite. According to [7], the chlorites mostly correspond to chamosite, and only 10% corresponds to clinochlore. Kaolinite and chlorite intergrowths were observed by [7] in the Carboniferous deposits in south-western Poland. According to [66], the process of kaolinite being replaced by chlorites is characteristic for thick sedimentary series, where the chlorite content increases at the cost of kaolinite together with the increase of the burial depth and temperature. The authors of [67] are of the opinion that the process of kaolinite chloritization may begin at 90–100 °C but is limited by the iron and magnesium amounts delivered from dissolved mafic minerals and lithoclasts. The authors of [68] refer to a transformation of kaolinite to Mg- or Fe-chlorite in the conditions of deep burial to the reaction of kaolinite with Mg/Fe-rich carbonates, which could happen at ~150 °C.

The sideroplesite was the first carbonate mineral that crystallized in the eodiagenesis in a temperature range of 15–40 °C [69]. The formation of this mineral is connected with anoxic conditions and low concentration of dissolved sulfates in the deposits rich in reactive iron-containing minerals [52]. The dolomite precipitated at the mesodiagenetic stage, being followed by Fe/Mn-calcite, Fe-dolomite and ankerite. Fluid inclusion studies point to the crystallization of Fe/Mn-calcite in the most frequent range of 90–104 °C (up to 158–233 °C) and of Fe-dolomite/ankerite in the interval from 76.9 °C to 134.5 °C (at maximum 160 °C).

The crystallization of the authigenic quartz could have started in the eodiagenesis. The further development of the quartz cement continued in the mesodiagenesis. According to [70], the formation of quartz overgrowths is possible at very low temperatures, even at 40–60 °C. Such situation was, e.g., discussed by [71] in the Cambrian sandstones from the offshore Baltic area. In most sedimentary basins, the authigenic quartz was formed in the temperature range of 60–145 °C [72]. To that range and the mesodiagenetic origin fall the quartz overgrowths in the Devonian sequence analyzed by [73]. Homogenization temperatures of two-phase inclusions in the authigenic quartz point to its crystallization in temperatures around 120 °C (max. 228 °C).

As for sulfates, the barite crystallized presumably at the end of the eodiagenesis, while anhydrite formed at the late diagenetic stage, similar to the West Pomerania case referred by [74].

5.3.3. Other Processes

Replacement represents the process that results in carbonatic, locally anhydritic pseudomorphs after the feldspar grains and lithoclasts. Mostly replacing the matrix by the carbonates was observed.

Alteration corresponds to albitization, argilitization or chloritization. The lithoclasts of volcanic rocks were also chloritized. Muscovite is present due to illite recrystallization.

The diagenetic dissolution (mostly of feldspar grains) preceded their albitization. Traces of this process are faint under the polarizing microscope. The carbonate and anhydrite cements, and sometimes quartz grains and the lithoclasts, underwent the dissolution.

5.4. Paleotemperatures

The FI studies and the Raman analyses have shown that the Carboniferous deposits underwent diagenetic processes, reaching temperatures of about 160°C or even over 200 °C. The Raman spectra show a presence of characteristic bands in two intervals, namely of 1000–1800 cm^{-1} and 2400–3000 cm^{-1}, which points to a low coalification degree of the organic matter CM (Figure 9F).

Ref. [13] studied epigenetic veins and some cements in the Carboniferous rocks in the selected boreholes from the Wielkopolska region, i.e., their results could be partly compared with present data. The T_h values obtained for different minerals (quartz, anhydrite, ankerite, calcite) are quite high in the interval from 150 °C to 300 °C. Their detailed results match the results obtained in the present study well. For the diagenetic structures and veinlets in the Września IG 1 borehole (depth 4915.8 m), these authors obtained T_h = 126–132 °C (quartz); in the Siekierki IG 1 borehole (depth 4144.6 m), T_h = 130–140 °C (paragenesis calcite + gypsum + anhydrite); in the Siciny IG 1 borehole, T_h = 106–115 °C (calcite, depth 2341.2 m) and T_h = 122–146 °C (ankerite, depth 2313.6 m). The were relatively high temperatures of fluid inclusions in the minerals studied both at present and by [13]. The authors of [14] suggest that the paleogeothermal field of the Fore-Sudetic Monocline was generally uplifted.

The results of measurements of the vitrinite reflectance in boreholes in the study area correspond to the interval from 0.7% to 2.0% [75–77]. Paleotemperatures that occur in the deposits were 80–180 °C. However, locally, an increase of temperatures >200 °C could have occurred, which is reflected in some of the fluid inclusion results. This may point to a regional metamorphism of a very low degree. The temperature increase could have resulted from the late Variscan inversion and early Permian volcanism, and hydrothermal activity could be connected with these events [14,78].

The studies of the Carboniferous deposits in the Fore-Sudetic Monocline of [7] point to high temperatures that were reached. According to the author cited, who used several varieties of chlorite geothermometers based on the tetrahedral aluminum, temperatures of formation of authigenic chlorites were 240–290 °C. Some researchers, however, are of the opinion that chlorite geothermometry should be applied carefully, with other verifying methods always (e.g., [79]). Still, according to [7], the temperatures obtained are concordant with the results of the measurements of vitrinite reflectance of 210–330 °C at the maximum. Such thermal conditions correspond to the anchizone and the lower range of the epizone in the Kübler's classification [80] and the very low or low metamorphism in the Winkler's classification [81].

6. Conclusions

1. Sandstones, mudstones and claystones are the Carboniferous clastic deposits in the studied area. The sandstones, mostly very fine- and fine-grained, are represented by wackes and locally arenites (sublithic or lithic, rare subarkosic, locally quartz arenites). A portion of the deposits contains abundant volcanic material (among others, the Katarzynin 2 borehole). The clayey-siliceous-ferruginous matrix and cements constitute the cement of the sandstones. Authigenic clay minerals (chlorites, mixed-layered illite/smectite minerals and illite), carbonates, authigenic quartz and anhydrite are the most significant cements. Numerous veins filled with carbonate minerals, quartz and anhydrite are present in the Carboniferous deposits.
2. The dolomite, Fe-dolomite/ankerite and Fe/Mn-calcite are the most significant carbonates. The $\delta^{13}C$ values for the carbonates point to their formation in the zone of

the microbiological methanogenesis and thermal decarboxylation. The calcite formed in the temperature range of 90–165 °C from pore waters of $\delta^{18}O_{SMOW}$ from about −4‰ to ~4‰ and salinity of ~4 wt. per cent NaCl eq. The Fe-dolomite/ankerite precipitated at temperatures from ~77°C to ~160 °C from pore waters of $\delta^{18}O_{SMOW}$ from 0 to ~10‰ (mostly >4‰) and salinity ~4.6 wt. per cent NaCl eq.

3. Homogenization temperatures of AQFI for carbonate minerals and the authigenic quartz in the Carboniferous deposits fall into the interval of 77 °C to 233 °C. The fluid salinity varies with respect to the mineral filling the veins or forming the cement. It changes as follows: calcite 0–14 wt. % NaCl eq., Fe-dolomite/ankerite ~5 wt. % NaCl eq. and quartz ~4 wt. % NaCl eq. The density of fluids in AQFI is close to 1 g/cm^3. The analyses of AQFI conducted suggest a presence of complex fluids in the inclusions, e.g., H_2O-NaCl-$CaCl_2$-$MgCl_2$ and mixed systems of brines with a gas of a methane composition, possibly admixed by nitrogen/CO_2/H_2S.
4. Two-phase inclusions with vapor containing the methane with nitrogen were observed in the minerals from the Zakrzyn IG 1 borehole (at depths of 3039 m and 3074 m). The mono-phase inclusions (HCFI), no fluorescence or dull blue fluorescence were noticed in the Katarzynin 2 (2510.6–2639.5 m) and Objezierze IG 1 (4895.7 m) boreholes. These inclusions contain mostly methane.
5. Brine-methane co-occurrence in inclusions in Fe-dolomite/ankerite and calcite points to a common brine-hydrocarbon front and may indicate that the precipitation of these minerals took place during the migration of these fluids.
6. Based on the brine-methane co-occurrence in the inclusions, the trapping conditions of fluids were estimated to be ~850–920 bars and 185–210 °C (vein calcite, Zakrzyn IG 1) and ~1140 bars and 220 °C (Fe-dolomite/ankerite Katarzynin 2).
7. The Carboniferous deposits in the Katarzynin 2 borehole (depth 2638.6 m; 2588.45 m) may be interpreted as the most prospective for the search for hydrocarbons. They are the only deposits in the borehole section where hydrocarbon inclusions occur.
8. The Carboniferous sediments were influenced by the eo- and mesodiagenetic processes. The maximum diagenetic temperature is estimated to be ~160 °C. Locally, however, a temperature increases even >200 °C could have occurred, which is supported by some fluid inclusion results, Raman analyses of the organic matter and the chlorite geothermometry. This could point to local, regional metamorphism of a very low degree.

Author Contributions: Conceptualization, K.J.-S. and A.K.; methodology, K.J.-S., A.K., M.K., K.W.; software, K.J.-S., A.K., M.K.; validation, K.J.-S. and A.K.; formal analysis, K.J.-S. and A.K.; investigation, K.J.-S., A.K., M.K., K.W.; resources, K.J.-S., A.K., M.K., K.W.; writing—original draft preparation, K.J.-S. and A.K.; writing—review and editing, K.J.-S. and A.K.; visualization, K.J.-S. and A.K.; supervision, K.J.-S. and A.K. All authors have read and agreed to the published version of the manuscript.

Funding: This research received no external funding.

Acknowledgments: The present studies are based on the results of investigations performed in 2016–2018 by PGI-NRI in the frame of the project "Recognition of prospective zones for the occurrence of unconventional hydrocarbon reservoirs in Poland. Continuous task of Polish Geological Survey" financed by the National Fund for Environmental Protection and Water Management. The authors thank M. Sikorska-Jaworowska for CL studies, L. Giro for SEM analyses and W. Narkiewicz and M. Dohnalik with their research team for XRD analyses. M. Joachimski is acknowledged for oxygen and carbon isotopic analyses. T. Toboła is thanked for providing the Raman analyses results. Two anonymous reviewers are thanked for their detailed and constructive comments and suggestions that helped the authors improve the manuscript. Important language corrections were made by Pete Modreski, to whom the authors express their cordial thanks. Special thanks are directed to Georgia Pe-Piper, who conducted the scientific review and final correction of the revised manuscript. The authors are greatly indebted to her for her kindness and professionalism.

Conflicts of Interest: The authors declare no conflict of interest.

References

1. Cebulak, S. Results of petrographic studies. Carboniferous. In *Więcki IG 1, Profile Głęb. Otw. Wiert. Państw. Inst. Geol.*; Grodzicka-Szymanko, W., Ed.; Wydawnictwa Geologiczne: Warsaw, Poland, 1976; Volume 35, pp. 47–57. (In Polish)
2. Butkiewicz, M. Petrographic analysis of the Carboniferous deposits. In *Documentation of deep borehole Września IG 1*; Sokołowski, J., Ed.; Archive materials, Narod. Arch. Geol. PIG-PIB: Warsaw, Poland, 1977; pp. 170–181. (In Polish)
3. Kłapciński, J.; Lorenc, S. Petrographic differentiation of the sub-Permian sedimentary complex in the western part of the Fore-Sudetic Monocline and the Żary perycline. *Acta Univ. Wratisl. Pr. Geol. Miner.* **1984**, *9*, 3–18. (In Polish)
4. Speczik, S. Ore mineralization in the basement Carboniferous rocks of the Fore-Sudetic Monocline (SW Poland). *Geol. Sudet.* **1979**, *14*, 77–119, (In Polish with English Summary).
5. Speczik, S.; Wiszniewska, J. Processes of diagenesis and epigenesis in Carboniferous rocks of the northern part of the bedrock of the Fore-Sudetic Monocline on the example of Września lG 1 profile. *Kwart. Geol.* **1981**, *25*, 265–285, (In Polish with English Summary).
6. Barczuk, A.; Speczik, S. Diagenetic processses in the Carboniferous deposits in the northern part of the Fore-Sudetic Monocline. *Arch. Miner.* **1981**, *37*, 67–92. (In Polish)
7. Krzemiński, L. Provenance of carboniferous sandstones from the variscan foreland basins in southwestern Poland and Moravia (in Polish with English summary). *Biul. Państw. Inst. Geol.* **2005**, *417*, 27–108.
8. Kozłowska, A.; Kuberska, M. The Lower Carboniferous sandstones in the Wielkopolska-Silesia zone prospective for tight gas exploration (preliminary studies) (in Polish with English summary). *Biul. Państw. Inst. Geol.* **2015**, *464*, 49–60. [CrossRef]
9. Poprawa, P.; Kiersnowski, H. Potential for shale gas and tight gas exploration in Poland (in Polish with English summary). *Biul. Państw. Inst. Geol.* **2008**, *429*, 145–152.
10. Podhalańska, T.; Adamczak-Biały, T.; Becker, A.; Dyrka, I.; Feldman-Olszewska, A.; Głuszyński, A.; Grotek, I.; Janas, M.; Jarmołowicz-Szulc, K.; Jachowicz, M.; et al. Recognition of the Zones Prospective for Unconventional Hydrocarbon Deposits in Poland. In *Continous PGS Project, Stage I, Final Report*; Archive materials, Narod. Arch. Geol. PIG-PIB: Warsaw, Poland, 2016; No 4878/2016. (In Polish)
11. Podhalańska, T.; Adamczak-Biały, T.; Becker, A.; Dyrka, I.; Feldman-Olszewska, A.; Głuszyński, A.; Grotek, I.; Janas, M.; Jarmołowicz-Szulc, K.; Jachowicz, M.; et al. Recognition of the Zones Prospective for Unconventional Hydrocarbon Deposits in Poland. In *Continous PGS Project, Stage II, Final Report*; Archive materials, Narod. Arch. Geol. PIG-PIB: Warsaw, Poland, 2018; No 9051/2019. (In Polish)
12. Wójcicki, A.; Kiersnowski, H.; Dyrka, I.; Adamczak-Biały, T.; Becker, A.; Głuszyński, A.; Janas, M.; Kozłowska, A.; Krzemiński, L.; Kuberska, M.; et al. *Prognostic Resources of the Earth Gas in Selected Compact Reservoir Rocks in Poland*; Archive materials, Polish Geol. Inst.—NRI: Warsaw, Poland, 2014. (In Polish)
13. Speczik, S.; Kozłowski, A. Fluid inclusion study of epigenetic veinlets from the Carboniferous rocks of the Fore-Sudetic monocline (SW Poland). *Chem. Geol.* **1987**, *61*, 287–298. [CrossRef]
14. Poprawa, P.; Grotek, I.; Żywiecki, M.M. Impact of the Permian magmatic activity on the thermal maturation of the Carboniferous sediments in the outer variscan orogen (SW Poland). *Min. Soc. of Poland Sp. Pap.* **2005**, *26*, 253–259.
15. Roedder, E. Reviews in Mineralogy, Fluid Inclusions. *Miner. Soc. Amer.* **1984**, *12*, 1–254.
16. Shephard, T.J.; Rankin, A.H.; Alderton, D.H.M. *A Practical Guide to Fluid Inclusion Studies*; Blackie: New York, NY, USA, 1985.
17. Goldstein, R.H. Fluid inclusions in sedimentary and diagenetic systems. *Lithos* **2001**, *55*, 159–193. [CrossRef]
18. Goldstein, R.H. Re-equilibration of fluid inclusions in low temperature calcium-carbonate cements. *Geology* **1986**, *14*, 792–795. [CrossRef]
19. Goldstein, R.H.; Reynolds, T.J. Systematics of fluid inclusions in diagenetic minerals. *SEPM Short Course* **1994**, *31*, 199.
20. Unrug, R.; Dembowski, Z. Diastrophic and sedimentary evolution of the Moravia-Silesia Basin. *Ann. Soc. Geol. Pol.* **1971**, *41*, 119–168. (In Polish with English Summmary)
21. Bojkowski, K.; Dembowski, Z. Paleogeography of the Carboniferous deposits in the Lublin Coal Basin on the background of the Carboniferous paleogeography of Poland. In *The Carboniferous of the Lublin Coal Basin, Pr. Inst. Geol.*; Dembowski, Z., Porzycki, J., Eds.; Wydawnictwa Geologiczne: Warsaw, Poland, 1988; Volume 122, pp. 18–26, (In Polish with English Summary).
22. Mazur, S.; Aleksandrowski, P.; Turniak, K.; Krzemiński, L.; Mastalerz, K.; Rundach, A.; Górecka-Nowak, A.; Kurowski, L.; Krzywiec, P.; Żelaźniewicz, A.; et al. Uplift and late orogenic deformation of the Central European Variscan belt as revealed by sediment provenance and structural record in the Carboniferous foreland basin of western Poland. *Inter. J. Earth Sci. (Geol. Rundsch.)* **2010**, *99*, 47–64. [CrossRef]
23. Mierzejewski, M. Tectonics. In *Lithology, Petrograhy, Geochemistry, Heavy Minerals, Stratigraphy and Tectonics of the Sub-Permian Basement in the Eastern Part of the Fore-Sudetic Monocline*; Kłapciński, L., Ed.; Archive materials, Arch. Uniw. Wr., ZOOGGN Geonafta: Warsaw, Poland, 1975. (In Polish)
24. Jarosiński, M. Tectonic and geodynamic studies in the Paproć 29 borehole. In *Analysis of the Carboniferous Deposits in the Recognition Paproć 29 Borehole (Anex to the Project: "Geological Structure of the Variscides in the Basement of the Fore-Sudetic Monocline")*; Lipiec, M., Ed.; Archive materials, Narod. Arch. Geol. PIG-PIB: Warsaw, Poland, 1997; No 134191. (In Polish)
25. Aleksandrowski, P.; Kurowski, L.; Mazur, S. Structure and sedymentology of the Carboniferous complex of the Variscan externides in the area of the Fore-Sudetic Monocline based on the geophysical log data and drilling log material. Report II. In *Paleozoic Accretion of Poland*; Nawrocki, J., Ed.; Archive materials, Narod. Arch. Geol. PIG-PIB: Warsaw, Poland, 2003. No 2870/05. (In Polish)

26. Cebulak, S.; Dembowski, Z. Results of stratigraphic and lihtologic research. In *Marcinki IG 1, Profile Głęb. Otw. Wiert. Państw. Inst. Geol.*; Gajewska, I., Ed.; Wydawnictwa Geologiczne: Warsawm Poland, 1973; Volume 8, pp. 19–39. (In Polish)
27. Górecka-Nowak, A. Palynological data from the Siciny IG 1 and Marcinki IG 1 boreholes and their significance to the interpretation of the Carboniferous succession of SW Poland. *Geol. Quart.* **2009**, *53*, 167–186.
28. Żelichowski, A. Lithological associations in the Carboniferous in Poland (in Polish with English summary). *Prz. Geol.* **1983**, *31*, 342–350.
29. Waksmundzka, M. Chapter 6. Carboniferous. In *Petroleum Geological Atlas of the Southern Permian Basin Area*; Doornenbal, H., Stevenson, A., Eds.; EAGE Publ.: Houten, The Netherlands, 2010; pp. 81–99.
30. Pettijohn, F.J.; Potter, P.E.; Siever, R. *Sand and Sandstone*; Springer: New York, NY, USA, 1972.
31. Środoń, J.; Drits, V.A.; McCarty, D.K.; Hsieh, J.C.C. Quantitative analysis of clay-bearing rocks from random preparations. *Clay Clay Min.* **2001**, *49*, 514–528. [CrossRef]
32. Rietveld, H.M. A profile refinement method for nuclear and magnetic structures. *J. Appl. Crystal.* **1969**, *2*, 65–71. [CrossRef]
33. Joachimski, M.; GeoZentrum Nordbayern at the Friedrich-Alexander University Erlangen-Nürnberg, Germany. Personal Communication, 2020.
34. Kim, S.T.; Mucci, A.; Taylor, B.E. Phosphoric acid fractionation factors for calcite and aragonite between 25 and 75 °C: Revisited. *Chem. Geol.* **2007**, *246*, 135–146. [CrossRef]
35. Rosenbaum, J.; Sheppard, S.M. An isotopic study of siderites, dolomites and ankerites at high temperatures. *Geochim. Cosmochim. Acta* **1986**, *50*, 1147–1150. [CrossRef]
36. Jarmołowicz-Szulc, K. Fluid inclusion systematics in the filling of a pore space in the Palaeozoic sedimentary rocks in the Polish Lowlands. *Prz. Geol.* **1999**, *47*, 542–546, (In Polish with English Summary).
37. Reynolds, J.T. Synflinc Standards Manual. Denver, CO, USA, 2 May 1993.
38. Goldstein, R.H. Petrographic analysis of fluid inclusions. *Fluid Incl. Anal. Interpret. Mineral. Assoc. Can. Short Course* **2003**, *32*, 9–54.
39. Bakker, R.J. Package FLUIDS. Computer programs for analysis of fluid inclusion data and for modeling bulk fluid properties. *Chem. Geol.* **2003**, *194*, 3–23. [CrossRef]
40. Brown, P.E. FLINCOR: A microcomputer program for the reduction and investigation of fluid inclusion data. *Am. Min.* **1989**, *74*, 1390–1393.
41. Bakker, R.J.; Brown, P.E. Computer modeling in fluid inclusion research. *Fluid Incl. Anal. Interpret. Mineral. Assoc. Can. Short Course* **2003**, *32*, 175–203.
42. Bodnar, R.J. Interpretation of data from aqueous-electrolyte fluid inclusions. *W Fluid Incl. Mineral. Assoc. Can. Short Course* **2003**, *32*, 81–101.
43. Toboła, T. Raman spectroscopy of organic, solid and fluid inclusions in the Oldest Halite of LGOM area (SW Poland). *Spectrochim. Acta Part A Mol. Biomol. Spectrosc.* **2018**, *189*, 381–392. [CrossRef] [PubMed]
44. Dudok, I.V.; Jarmołowicz-Szulc, K. Hydrocarbon inclusions in vein quartz (the "Marmarosh diamonds" from the Krosno and Dukla zones of the Ukrainian Carpathians. *Geol. Quart.* **2000**, *44*, 415–423.
45. Jarmołowicz-Szulc, K.; Wołkowicz, K. *Analysis of Fluid Inclusions in the Objezierze IG 1, Zakrzyn IG 1, Katarzynin 2, Kalisz IG 1 and Siedliska IG 1, Równce 1, Łochów IG 1, Płońsk IG 2/2, Darżlubie IG1*; Archive materials, Nat. Geol. Arch.: Warsaw, Poland, 2018. (In Polish)
46. Kouketsu, Y.; Mizukami, T.; Mori, H.; Endo, S.; Aoya, M.; Hara, H.; Nakamura, D.; Wallis, S. A new approach to develop the Raman carbonaceous material geothermometer for low-grade metamorphism using peak width. *Island Arc.* **2014**, *23*, 33–50. [CrossRef]
47. Burke, E.A.J. Raman microspectrometry of fluid inclusions. *Lithos* **2001**, *55*, 139–158. [CrossRef]
48. Samson, I.; Anderson, A.; Marshall, D. (Eds.) *Fluid inclusions Analysis and Interpretation*; Mineralogical Association of Canada: Vancouver, Canada, 2003; Volume 32, pp. 175–203.
49. Jarmołowicz-Szulc, K.; Toboła, T. Microthermometric and Raman spectra studies in minerals in the Rabe vicinity (Carpathians)—An experimental practice. *Prz. Geol.* **2021**, *69*, 361–364. [CrossRef]
50. Jarmołowicz-Szulc, K. Remarks on use of Inclusions in Minerals in the Rocks of Hydrocarbon Fields. *Int. J. Petrochem. Sci. Eng.* **2018**, *3*, 00069. [CrossRef]
51. Jarmołowicz-Szulc, K. Application of fluid inclusions to petroleum basin recognition–a case study from Poland. *Minerals* **2021**, *11*, 500. [CrossRef]
52. Morad, S. Carbonate cementation in sandstones: Distribution patterns and geochemical evolution. *Spec. Publ. Int. Ass. Sediment.* **1998**, *26*, 1–26.
53. Friedman, I.; O'Neil, J. Compilation of stable isotope fractionation factors of geochemical interest. In *Data of Geochemistry*; Fleischer, M., Ed.; Professional Paper; U.S. Geological Survey: Reston, VA, USA, 1977; Volume 440-K, pp. 1–12.
54. Dutton, S.P.; Land, L.S. Meteoric burial diagenesis of Pensylvanian arkosic sandstones, Southwestern Anadarko Basin, Texas. *AAPG Bull.* **1985**, *69*, 22–38.
55. Longstaffe, F.J.; Ayalon, A. Hydrogen—Isotope geochemistry of diagenetic clay minerals from Cretaceous sandstones, Alberta, Canada: Evidence for exchange. *Appl. Geochem.* **1990**, *5*, 657–668. [CrossRef]

56. Fisher, R.S.; Land, L.S. Diagenetic history of Eocene Wilcox sandstones, South—Central Texas. *Geochim. Cosmochim. Acta* **1986**, *50*, 551–561. [CrossRef]
57. Choquette, P.W.; Pray, L.C. Geologic nomenclature and classification of porosity in sedimentary carbonates. *AAPG Bull.* **1970**, *54*, 207–220.
58. Worden, R.H.; Burley, S.D. Sandstone diagenesis: The evolution of sand to stone. *Sandstone Diagenesis Recent Anc.* **2003**, *4*, 3–44.
59. Mücke, A. Postdiagenetic ferruginization of rocks (sandstones, oolitic ironstones, kaolins and bauxites)—Including a comparative study of the reddening of red beds. *Dev. Sedimentol.* **1994**, *51*, 361–423.
60. Postma, D. Pyrite and siderite formation in brackish and freshwater swamp sediments. *Am. J. Sci.* **1982**, *282*, 1151–1183. [CrossRef]
61. Osborn, M.; Haszeldine, R.S.; Fallick, A.E. Variation in kaolinite morphology with growth temperature in isotopically mixed pore—fluids, Brent Group, UK North Sea. *Clay Miner.* **1994**, *29*, 591–608. [CrossRef]
62. Ehrenberg, S.N.; Aagaard, P.; Wilson, M.J.; Fraser, A.R.; Duthie, D.M.L. Depth-dependent transformation of kaolinite to dickite in sandstones of the Norwegian Continental Shelf. *Clay Miner.* **1993**, *28*, 325–352. [CrossRef]
63. Hartmann, B.H.; Juhász-Bodnár, K.; Ramseyer, K.; Matter, A. Effect of Permo-Carboniferous climate on illite-smectite, Haushi Group, Sultanate of Oman. *Clays Clay Miner.* **1999**, *47*, 131–143. [CrossRef]
64. Środoń, J. Clay minerals in diagenetic processes. *Prz. Geol.* **1996**, *44*, 604–607, (In Polish with English Summary).
65. Bjørlykke, K. Clay mineral diagenesis in sedimentary basins—A key to the prediction of rock properties. Examples from the North Sea Basin. *Clay Miner.* **1998**, *33*, 15–34. [CrossRef]
66. Weaver, C.E.; Highsmith, P.B.; Wampler, J.M. Chlorite. In *Shale-Slate Metamorphism in the Southern Appalachians*; Weaver, C.E., Ed.; Elsevier: Amsterdam, The Netherlands, 1984; pp. 99–139.
67. Bjørlykke, K.; Aagard, P. Clay minerals in North Sea sandstones. In *Origin, Diagenesis and Petrophysics of Clay Minerals in Sandstones*; Hauseknecht, D.W., Pittman, E.D., Eds.; Special Publication (SEPM); AAPG: Tulsa, OK, USA, 1992; Volume 47, pp. 65–80.
68. Hutcheon, I.; Oldershaw, A.; Ghent, E.D. Diagenesis of Cretaceous sandstones of the Kootenay Formation at Elk Valley (southestern British Columbia) and Mt Allan (southwestern Alberta). *Geochim. Cosmoch. Acta* **1980**, *44*, 1425–1435. [CrossRef]
69. Backer, J.C.; Kassan, J.; Hamilton, P.J. Early diagenetic siderite as indicator of depositional environment in the Triassic Rewan Group, Southern Bowen basin, eastern Australia. *Sedimentology* **1995**, *43*, 77–88. [CrossRef]
70. Grant, S.M.; Oxtoby, N.H. The timing of quartz cementation in Mesozoic sandstones from Haltenbanken, offshore mid-Norway: Fluid inclusion evidence. *J. Geol. Soc.* **1992**, *149*, 479–482. [CrossRef]
71. Jarmołowicz-Szulc, K. Fluid inclusion studies in quartz cements in the Middle Cambrian sandstones in the Łeba Block in the Baltic Sea—Diagenetic, isotope and geochemical implications. *Biuletyn Państw. Inst. Geol.* **2001**, *399*, 1–83.
72. Walderhaug, O. Temperatures of quartz cementation in Jurasic sandstones from the Norwegian continental shelf—Evidence from fluid inclusions. *J. Sed. Res.* **1994**, *64*, 311–323.
73. Khalifa, M.A.; Mansurbeg, H.; Morad, D.; Al-Aasm, I.S.; Spirov, P.; Ceriani, A.; de Ross, L.F. Quartz and Fe-dolomite cements record shifts in formation-water chemistry and hydrocarbon migration in Devonian shoreface sandstones, Ghadamis Basin, Libya. *J. Sed. Res.* **2018**, *88*, 38–57. [CrossRef]
74. Kozłowska, A. Diagenesis and pore space evolution in Pennsylvanian sandstones from Western Pomerania. *Biul. Państw. Inst. Geol.* **2008**, *430*, 1–28, (In Polish with English Summary).
75. Nowak, G. Petrology of the dispersed organic matter in late Paleozoic sedimentary rocks of SW Poland. *Cuprum* **2003**, *4*, 1–221, (In Polish with English Summary).
76. Nowak, G. Petrology of dispersed organic matter in Carboniferous rocks of the Fore-Sudetic Homocline basement. *Prz. Geol.* **2016**, *64*, 1005–1007.
77. Botor, D.; Papiernik, B.; Maćkowski, T.; Reicher, B.; Kosakowski, P.; Machowski, G.; Górecki, W. Gas generation in Carboniferous source rocks of the variscan foreland basin: Implications for a charge history of Rotliegend deposits with natural gases. *Ann. Soc. Geol. Pol.* **2013**, *83*, 353–383.
78. Karnkowski, P. Origin and evolution of the Polish Rotliegend basin. *Pol. Geol. Inst. Spec. Pap.* **1999**, *3*, 1–93.
79. De Caritat, P.; Hutcheon, I.; Walshe, J.L. Chlorite geothermometry: A review. *Clays Clay Miner.* **1993**, *41*, 219–239. [CrossRef]
80. Kisch, H.J. Correlation between indicators of very low-grade metamorphism. In *Low Temperature Metamorphism*; Frey, M., Ed.; Blackie and Son Ltd: Glasgow, UK, 1987; pp. 227–300.
81. Winkler, H.G.F. *Petrogenesis of Metamorphic Rocks*; Springer: New York, NY, USA, 1979.